van Helden *et al.*
Journal of Applied Volcanology (2024) 13:6
https://doi.org/10.1186/s13617-024-00145-w

Journal of Applied Volcanology

METHODOLOGY

Open Access

The influence of vesicularity on grain morphology in basaltic pyroclasts from Mauna Loa and Kīlauea volcanoes

Kira M. van Helden[1*], Johanne Schmith[2] and Drew T. Downs[2]

Abstract

Vesicularity of individual pyroclasts from airfall tephra deposits is an important parameter that is commonly measured at basaltic volcanoes. Conventional methods used to determine pyroclast vesicularity on a large number of clasts has the potential to be time consuming, particularly when rapid analysis is required. Here we propose dynamic image analysis on two-dimensional (2D) projection shapes of crushed pyroclasts from tephra deposits as a new method to estimate vesicularity. This method relies on the influence of vesicles and uses grain morphology as a proxy for vesicle size and abundance. Pyroclasts from a variety of basaltic tephra deposits from the volcanoes of Mauna Loa and Kīlauea were analyzed. Vesicularities between 52–98% were measured via nitrogen-gas pycnometry. The same pyroclasts were then crushed and sieved, and their grain shapes measured using dynamic image analysis on a CAMSIZER®. This yields values for the mean sphericity, elongation, compactness, and Krumbein roundness of the grains. Our data show that grains become increasingly irregular with increasing vesicularity, with the degree of correlation between shape parameters and vesicularity depending on the size of measured grains. Shape irregularities in small grains (60–250 µm) are mostly area-based, with elongation being the best vesicularity indicator, whereas shape irregularities in large grains (250–700 µm) are mostly perimeter-based, with Krumbein roundness as the best vesicularity indicator. Using mean shape parameter values with all grain sizes included, grain elongation is the most well-correlated shape parameter with vesicularity, with the best fitted model explaining 76% of variation in the observations. Microscope images of thin sections of intact pyroclasts, as well as from crushed pyroclasts, were analyzed using CSDCorrections 1.6 software in ImageJ to find local vesicularity, vesicle size, grain size, grain elongation, and vesicle spatial distribution by stereological conversion. Observed correlation between grain shape and vesicularity can be explained by the local effect of vesicles on the shape of the solid structure in between those vesicles. Grain shape depends not only on vesicularity, but also on vesicle to grain size ratio and the spatial distribution of vesicles. The influence of vesicles on grain shape is best captured by grains with the size of the solid structure in between vesicles, which generally increases with decreasing vesicularity. Dynamic image analysis is a useful tool to quickly gauge vesicularity, which could be used in near-real-time during an eruption response. However, this method is best suited for highly vesicular (> 80%) basaltic pyroclasts from tephra deposits with few microlites and phenocrysts. Further research on crushing techniques, optimum grain size for shape measurements, and Krumbein roundness measurements for the grain size range of 250–700 µm might enable application of this method to lower vesicularity pyroclasts.

Keywords Tephra, Vesicularity, Dynamic image analysis, Grain size, Grain shape

*Correspondence:
Kira M. van Helden
k.m.vanhelden@students.uu.nl
Full list of author information is available at the end of the article

Introduction

Hawaiian volcanoes are known for their low-explosivity 'Hawaiian style' eruptions that produce fluid lava flows and associated spatter, scoria, and tephra deposits from lava fountains. However, widespread basaltic airfall tephra deposits (i.e., pyroclasts of ash, lapilli, and bombs) surrounding the summits of Kīlauea and Mauna Loa (Island of Hawai'i) indicate a significant amount of more moderate to highly explosive volcanism (Volcanic Explosivity Index of 1–3) that has occurred in the past (e.g., Swanson et al. 2012, 2014; Swanson and Houghton 2018; Trusdell et al. 2018; Schmith and Swanson 2023). Understanding vesicularity, grain size and shape, and microlite content of past eruptive cycles in explosive versus effusive episodes is important for characterizing conduit and eruptive dynamics of future activity (e.g., Parfitt 2004; Mueller et al. 2011; Stovall et al. 2011, 2012; Parcheta et al. 2013; Gonnermann 2015; Cáceres et al. 2020; Colombier et al. 2021).

The explosive eruptions of Kīlauea and Mauna Loa produced pyroclasts of variable vesicularity, some of which reach > 95% vesicles (reticulite). Pyroclast vesicularity is an important parameter that varies with eruption style and provides insight into magmatic fragmentation processes (e.g., Houghton and Wilson 1989; Vergniolle 1996; Mueller et al. 2011; Stovall et al. 2011, 2012; Alfano et al. 2012; Parcheta et al. 2013; Gonnermann 2015; Colombier et al. 2017a, 2017b, 2018; Pisello et al. 2023). While vesicularity data can help assess hazards during eruption response efforts, it is typically not straight-forward as (1) there is generally overlap in the porosity of basaltic pyroclasts that are produced by different eruptive styles and (2) porosity/vesicularity can be modified after fragmentation (e.g., Stovall et al. 2011) and/or by densification from surface tension and permeable outgassing of bubbles near the margins of pyroclasts (e.g., Namiki et al. 2018). Here, a new method is proposed to estimate the vesicularity by linking it to grain morphology (i.e., shape) and size of crushed pyroclasts of past eruptions in order to better understand future activity.

A correlation exists between vesicularity and tephra grain shape, with tephra grain morphology commonly affected by the presence of vesicles (Liu et al. 2015; Schmith et al. 2017; Mele et al. 2018; Mele and Dioguardi 2018). Grain morphology data are routinely acquired to support interpretation of eruptive mechanisms, plume dispersal, and related tephra hazards (Pyle 1989; Parfitt 1998; Parfitt and Wilson 1999; Mastin et al. 2009; Saxby et al. 2018). The question is whether grain shape parameters acquired using automatic dynamic image analysis can also give direct quantitative constraints on the vesicularity of pyroclasts within tephra deposits, and therefore on fragmentation processes and eruptive styles.

Vesicularity and magmatic fragmentation

During an explosive eruption, magma that consists of liquid melt, dispersed gas bubbles, and crystals ascends toward the surface and develops into a gas phase with dispersed magma fragments: a process called magmatic fragmentation (e.g., Parfitt 2004; Mueller et al. 2011; Cashman and Scheu 2015; Gonnermann 2015). While a simplistic view for low-viscosity basaltic magmas, if vesiculation is rapid enough to prevent individual bubbles from coalescing and prevent gas from escaping, fragmentation occurs (Rust and Cashman 2011), and a continuous gas phase that contains dispersed magma fragments is formed. However, there are different escape pathways for gas from basaltic magmas, such as (1) decoupled flow where gas and melt rise at different velocities with fragmentation occurring by bubble bursting, and (2) coupled flow where gas escapes via bubble coalescence (Vergniolle and Jaupart 1986, 1990; Vergniolle 1996). Dispersed small bubbles coupled to the magma that are fragmented and air quenched form pyroclasts, and for smaller pyroclasts that are quenched without significant post-fragmentation vesiculation, coalescence, or relaxation, their vesicles preserve the fragmentation history of the magma (Cashman and Scheu 2015).

Previous studies on pyroclast vesicularity, and associated pyroclast characteristics, have yielded insights into degassing processes, fragmentation mechanisms, and eruption style parameters, such as bubble nucleation, bubble coalescence, bubble rise rate, magma rise rate, and magma discharge rate (e.g., Self and Sparks 1978; Vergniolle and Jaupart 1986, 1990; Houghton and Wilson 1989; Vergniolle 1996; Mangan and Cashman 1996; Parfitt 2004; Mueller et al. 2011; Stovall et al. 2011, 2012; Alfano et al. 2012; Parcheta et al. 2013; Burgisser and Degruyter 2015; Cashman and Scheu 2015; Gonnermann 2015; Colombier et al. 2017a, 2017b, 2018, 2021; Pisello et al. 2023). Bubble formation in low-viscosity basaltic magmas is poorly understood because high temperature experiments are needed to produce a representative melt (Baker et al. 2012). Furthermore, the high eruption temperatures of basaltic magmas may result in longer durations between eruption and quenching. Therefore, studies of fragmentation processes of low-viscosity basaltic magmas are limited to a small subset of pyroclasts and numerical modeling of analogue materials (Vergniolle and Jaupart 1990; Alidibirov and Dingwell 1996; Parfitt 2004; Alfano et al. 2012; Oppenheimer et al. 2020; Colombier et al. 2020, 2021, 2023).

Grain morphology

Grain morphology, an important indicator of fragmentation mechanisms, is partly controlled by its constituent bubbles and crystals, and itself helps control the dispersal characteristics of wind-blown tephra in explosive eruptions. Additionally, grain morphology can be used to distinguish between dry magmatic eruptions (i.e., fragmentation from volatile exsolution) and phreatomagmatic eruptions (i.e., fragmentation from interaction between magma and external water), or a combination of the two, due to the relationship between fragmentation processes and geometries (Heiken 1972; Murtagh and White 2013; Schmith et al. 2017; Figueiredo et al. 2022; Ross et al. 2022).

Liu et al. (2015) showed a correlation between grain solidity, grain diameter, vesicle number and diameter in volcanic ash. Solidity is the ratio between grain area and area of the convex hull of the grain. This correlation shows that grains with higher numbers of vesicles, or larger vesicles, are more irregular than grains with fewer or smaller vesicles. A similar observation was made by Schmith et al. (2017) from studies on grain shapes of basaltic ash from several Icelandic eruptions. Additionally, Mele et al. (2018) demonstrated a correlation between vesicularity and sphericity in pyroclasts from tephra deposits that have compositions of trachyte, trachybasalt, and tephritic-phonolite. It is clear that pyroclasts with higher vesicularities tend to generate more irregular ash grains; that is grain shape/morphology and vesicularity that are interconnected (Guimarães et al. 2019).

Mele and Dioguardi (2018) showed that for highly vesicular pyroclasts, the shape of a grain depends on its size. Their study reported a parabolic trend between sphericity and size, with grains that are slightly larger than the largest vesicles being the most irregular in shape. Grains that are smaller than the largest vesicles are more spherical because they are situated in the solid structure between vesicles, so that vesicles do not influence surface irregularities. Grains much larger than the largest vesicles are more spherical because the influence of a relatively small vesicle on the surface irregularity of a relatively large grain is small. As such, the best correlation between vesicularity and grain shapes should be obtained by measuring shape parameters for grains that are slightly larger than the largest vesicles.

Geological setting

This vesicularity and grain shape study focuses on eruptive products from the volcanoes of Mauna Loa and Kīlauea, an active hotspot basaltic system. Samples of several eruptions from ~ 1500 CE to June 2023 were used in this study to incorporate a broad range of eruption styles, each featuring distinct vesicularities and associated pyroclast characteristics (Table 1).

The five oldest samples used here are from the ~ 300 year period of explosive activity (Volcanic Explosivity Index of 1–3) of the Keanakāko‘i Tephra at Kīlauea (Swanson et al. 2012, 2014; Swanson and Houghton 2018; Schmith and Swanson 2023). For this study, we use the Keanakāko‘i Tephra stratigraphic classification of Swanson and Houghton (2018), with subdivisions (as single or clustered eruptive events) into units A through L5. Here we analyzed samples from units B, D, E, K1, and K2 that encompass a wide range of vesicularities as presented in Table 1 (for an overview and map of the Keanakāko‘i Tephra deposits see Swanson and Houghton 2018).

Additional samples from Mauna Loa and Kīlauea were used to supplement vesicularity ranges and eruptive styles that were not recorded by pyroclasts from the Keanakāko‘i Tephra. These included pyroclasts from near-vent tephra deposits of (1) the 1949 Mauna Loa summit eruption that deposited multiple lava flows and large amounts of pumiceous spatter ejecta (Macdonald and Orr 1950), (2) the 1959 very high fountaining eruption of Kīlauea Iki that filled Kīlauea Iki Crater with a lava lake and created the Pu‘upua‘i tephra cone (Richter et al. 1970), and (3) the September 2021 and June 2023 opening eruptive phases from Halema‘uma‘u that deposited reticulite pyroclasts around the summit of Kīlauea.

Methodology

Sampling

Samples were collected from the Keanakāko‘i Tephra, Mauna Loa 1949 tephra cone, Kīlauea Iki 1959 Pu‘upua‘i tephra cone, and Halema‘uma‘u September 2021 and June 2023 tephra deposits (Table 1; Fig. 1A–C). For each sampled tephra deposit, 20–30 pyroclasts were selected, dried at 65°C in an oven and cleaned using pressurized air.

Vesicularity analysis

Vesicularity of sampled pyroclasts was obtained from density and volume data using nitrogen-gas pycnometry. A dense rock equivalent (DRE) density of 2.9 g/cm^3 (dense basalt after Houghton and Wilson 1989) was assumed for all samples. The mass of each pyroclast was determined using the average of five measurements, and the dense rock volume (i.e., excluding vesicles) of the pyroclasts was calculated as follows:

$$V_{dense\ rock} = \frac{m_{clast}}{\rho_{DRE}}$$

The average pyroclast mass measured was 2.637 g, for which an unlikely deviation of 0.1 g/cm^3 in DRE density would lead to a deviation of 0.03 cm^3 for the calculated DRE volume.

Table 1 Characteristics of sampled eruptive products from the volcanoes of Mauna Loa and Kīlauea used for this study, ordered from youngest to oldest

Tephra deposit	Description	Eruption style	Age
Halemaʻumaʻu, June 2023 (Kīlauea)	Reticulite from opening eruptive phase of the June 2023 Halemaʻumaʻu eruption. Sampled at Kīlauea's summit during the first day of the eruption, during deposition	Lava lake and fountaining eruption within Halemaʻumaʻu Crater. The first lava fountain reached a height of ~ 100 m. Later, other vents opened that produced fountains up to ~ 10 m high	June 7, 2023
Halemaʻumaʻu, September 2021 (Kīlauea)	Reticulite sampled at Kīlauea's summit during the 2021 Halemaʻumaʻu eruption	Lava lake and fountaining eruption within Halemaʻumaʻu Crater. The highest lava fountain sustained a height of 20–25 m throughout the first night	September 29, 2021
Puʻupuaʻi surface (Kīlauea)	Tephra deposit that formed the Puʻupuaʻi tephra cone. Fluidal to pumiceous pyroclast textures (Stovall et al. 2011). Pyroclasts were picked from the deposit surface	High lava fountaining eruption of Kīlauea Iki (Richter et al. 1970)	November 15, 1959
Puʻupuaʻi (Kīlauea)	The same Puʻupuaʻi tephra deposit, but pyroclasts were picked from the subsurface	High lava fountaining eruption of Kīlauea Iki (Richter et al. 1970)	November 15, 1959
Mauna Loa 1949	Pumice deposit surrounding scoria cone on SSW rim of Mokuʻāweoweo caldera at the summit of Mauna Loa volcano (Macdonald and Orr 1950)	Large effusive eruption with lava fountaining	January 6, 1949
Keanakākoʻi Tephra (Kīlauea)			
Unit K2	Thin pumice airfall deposit overlying K1, previously known as the "eastern pumice". K1 and K2 are similar in appearance but differ chemically (Garcia et al. 2018). The lower part of K2 consists mostly of Pele's hair and tears, whereas the upper part contains pumice lapilli. The latter were sampled for this study	Lava fountaining event, erupted from the east side of Kaluapele (Swanson and Houghton 2018)	after 1823 CE
Unit K1	Pumice deposit, previously named the "golden pumice" (Sharp et al. 1987) after its gold-like color	High lava fountaining sequence (Biass et al. 2018)	between 1790 and 1823 CE
Unit E	Well-sorted scoria airfall deposit	Subplinian eruption (Swanson and Houghton 2018)	~ 1650 CE
Unit D	Fine to medium-grained ash, containing glassy pyroclasts that are mostly dense and blocky (Swanson and Houghton 2018; Schmith and Swanson 2023). Sampled pyroclasts are pumice lapilli of 2–3 cm diameter	Series of weak phreatomagmatic eruptions (Swanson and Houghton 2018; Schmith and Swanson 2023)	16th to early seventeenth century
Unit B	Reticulite bed surrounding Kīlauea Crater	Series of high (> 600 m) lava fountaining events (May et al. 2015)	~ 1500 CE

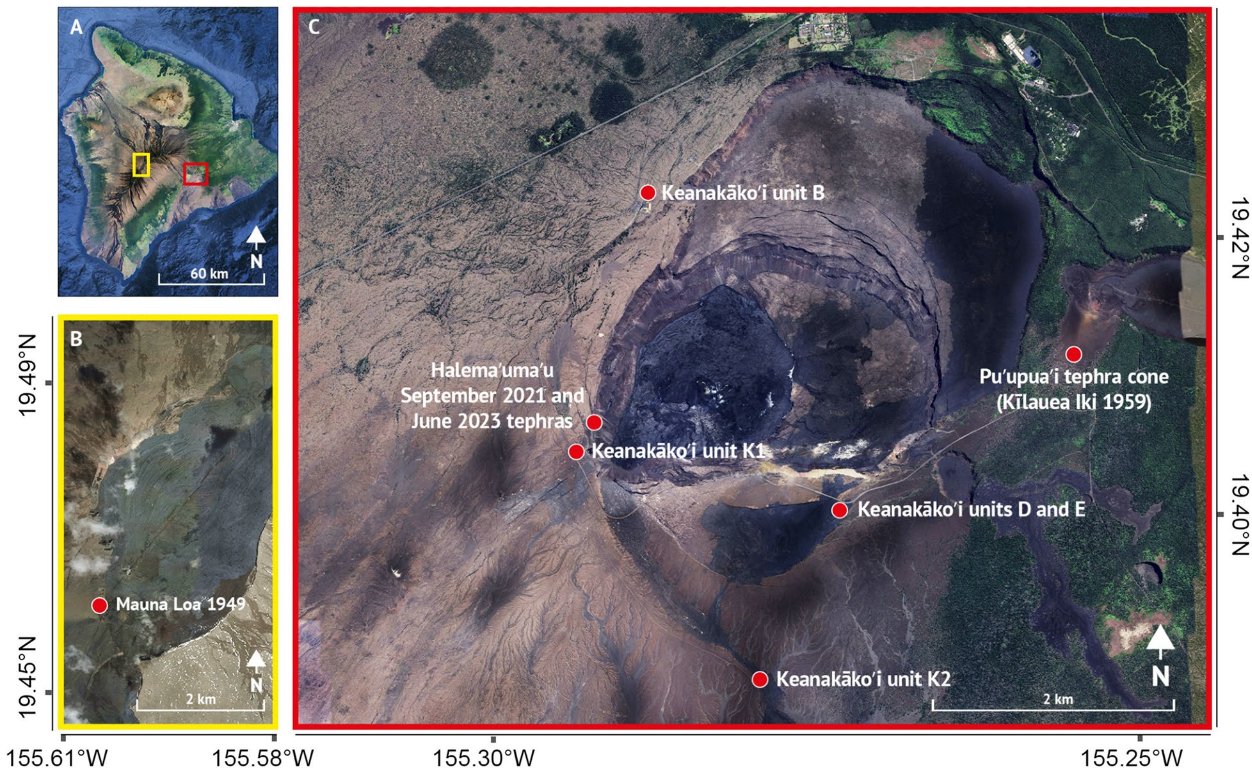

Fig. 1 Sampling locations. **A** Island of Hawai'i with the yellow box indicating the summit of Mauna Loa (**B**) and the red box indicating the summit of Kīlauea (**C**). Coordinates are given in the WSG84 coordinate system

Subsequently, the total pyroclast volume (i.e., including vesicles) V_{clast} was determined by sealing the pyroclast in hot glue, measuring the total volume with a pycnometer (using an Anton Paar Ultrapyc 5000), and subtracting the added hot glue volume. Any bubbles in the glue were punctured and re-glued where possible. Remaining bubbles were generally very small and scarce, so that unwanted errors in the measured volume were negligible. Values for V_{clast} were calculated from averages of ten volume measurements per sample, with a percent variance of 0.001–0.266. Verification measurements of known volumes were performed at the start of every lab session and yielded an average deviation of 0.039 cm^3.

Vesicularity of pyroclasts is defined as the percentage of the V_{clast} existing as vesicles:

$$vesicularity[\%] = \frac{V_{vesicles}}{V_{clast}} * 100\% = \frac{V_{clast} - V_{denserock}}{V_{clast}} * 100\%$$

Measurement errors can occur when clasts are not sealed properly, resulting in erroneously low vesicularities when gas enters vesicles during pycnometer measurements. To filter outliers due to failed sealing, all pyroclasts with a resulting vesicularity < 60%, which is unlikely for pyroclasts collected here (Houghton and Wilson 1989; May et al. 2015), were systematically glued and measured again. Notably, small errors due to gas entering a small part of the vesicles or glue occupying part of the vesicles in the outer part of the pyroclast might still be present, but likely even each other out. Any remaining errors in vesicularity were deemed negligible.

Grain shape analysis

After determining vesicularity, a subset of pyroclasts was selected that represent the full range of vesicularities within each of their host tephra deposits: 15 pyroclasts from Keanakāko'i unit B, 16 from Keanakāko'i unit D, 7 from Keanakāko'i unit E, 18 from Keanakāko'i unit K1, 18 from Keanakāko'i unit K2, 20 from Halema'uma'u 2021, 30 from Halema'uma'u 2023, 20 from Mauna Loa 1949, and 24 from Kīlauea Iki Pu'upua'i. The clasts were manually separated from their coating of glue, and then crushed by hand and sieved (to < 1180 μm). The two-dimensional (2D) shapes of the crushed grains were measured using a Microtrac CAMSIZER® X2. The instrument uses dynamic image analysis to obtain quantitative measurements of 2D grain shape parameters (Table 2) (Lo Castro and Andronico 2009; Lo Castro et al. 2009; Buckland et al. 2021; Schmith and Swanson 2023). A sample, consisting of a single crushed pyroclast, was imaged as it fell through the measurement field, where

Table 2 Dynamic image analysis shape parameters of interest

Parameter	Definition
Sphericity (SPHT)	The sphericity (SPHT) is a measure of the roundness of a grain. It depends on particle area (A) and perimeter (P): $SPHT = \frac{4\pi A}{P^2}$ For a perfect circle SPHT = 1, for all other shapes SPHT < 1
Elongation (aspect ratio) (b/l)	The aspect ratio (b/l) is a measure of the elongation of a grain. It is determined by the particle width/length ratio of the grain (the closer to 1, the more circular the grain): $\frac{b}{l} = \frac{x_{cmin}}{x_{Femax}}$ or $\frac{\text{particle width}}{\text{particle length}}$
Compactness (Compact)	The compactness (Compact) is a measure of the roundness of a grain. It depends on particle area (A) and particle length (x_{Femax}): $Compact = \frac{\sqrt{\frac{4A}{\pi}}}{l}$ For a perfect circle Compact = 1, for all other shapes Compact < 1
Krumbein roundness (RDNS)	The Krumbein roundness (RDNS) is a measure of the textural roughness of a grain. The parameter RDNS assigns a value between 0 and 1 to mimic the Krumbein roundness classification scheme (Krumbein 1941). Lower values mean higher roughness

two cameras with different resolutions recorded images of the grains at a frame rate of 300 frames per second. The CAMSIZER® software obtained the various shape parameters of individual grains on the images. The software determined the mean volumetric shape parameter values per pre-set grain size bin and for the entire sample (down to 62.5 µm) as a mean. Grains of < 62.5 µm were also measured, but these data are less reliable due to insufficient image resolution. The CAMSIZER® software, a dynamic image analysis system, automatically takes this influence of image resolution on the reliability of measurements of smaller grains into account when calculating mean values of grain size and shape parameters. The results yield a series of grain size and shape data for every pyroclast, which can be compared to their vesicularity.

Microscopic analysis

Thin section images were taken for a selection of deposits that represent the full range of vesicularities of the data: Keanakāko‘i Tephra units B, E, and K2, as well as the Pu‘upua‘i tephra, and Halema‘uma‘u 2021 tephra. These tephra deposits were selected based on their relatively narrow range of vesicularities within each individual deposit. Representative plain light microscopic images were made of (1) thin sections of two pyroclasts per selected deposit and (2) grains from crushed pyroclast samples from which vesicularities and grain shapes had been analyzed using pycnometry and the dynamic image analysis particle shape measurements. The images were taken with a Leica M125 C stereo microscope.

Image processing

Vesicles and grain boundaries in thin section images were outlined digitally in order to create binary images of vesicles surrounded by glass. These outlines were automatically created using ImageJ software (Schneider et al. 2012), visually inspected for errors and manually adjusted where necessary. The results were input into CSDCorrections 1.6 software (Sahagian and Proussevitch 1998; Higgins 2000, 2002). CSDCorrections was developed to analyze crystal size distributions in igneous and volcanic rocks. It performs stereological conversion of 2D microscopic images from object intersection data to volumetric size distributions, following methods described by Higgins (2000), based on Sahagian and Proussevitch (1998). The analysis and correction method can be applied to crystals, as well as to any other type of object in thin section images, such as any 2D intersection data, including those characterizing crystals, vesicles, or individual glass particles. The CSDCorrections software computes the total volume percentage, size distribution, elongation, and spatial distribution R of outlined objects (Table 3). This yields vesicularity and grain elongation; two parameters to be compared to the results from our pycnometry and dynamic image analysis grain shape data. CSDCorrections is not able to compute sphericity, compactness or Krumbein roundness, so grain elongation is the only parameter that can be used to compare shape irregularity measurements from CAMSIZER® to those from microscope images.

Accurate estimation of the vesicularity of entire pyroclasts requires analysis of a large number of images at different scales of multiple thin sections per pyroclast. For this type of analysis FOAMS (Shea et al. 2010a), a stereological conversion methods from Sahagian and Proussevitch (1998) similar to the CSDCorrections software, is commonly used. However, the aim of our microscopic analysis was not to estimate vesicularity of entire pyroclasts but to measure and visualize the local effect of vesicles on surrounding grain shapes, data that are used to support and explain the results from the dynamic image analysis grain shape measurements. For this reason, and for computational efficiency, quantifying the correlation between vesicularity and grain morphology

Table 3 Microscope image analysis parameters obtained from CSDCorrections 1.6 software

Parameter	Definition
Thin sections of intact pyroclasts	
Local vesicularity	Percentage of vesicles in small local part of rock captured by the microscopic image. Computed from the area of the measured image that is not occupied by glass, microlites, or (micro)phenocrysts
Mean vesicle size	Mean vesicle size, computed from vesicle size distribution in measured image area
Vesicle spatial distribution R	Measure of the average distance between vesicles. Computed as the ratio between observed and predicted distances between the centers of nearest neighboring objects (Jerram et al. 1996), in this case applied to vesicles. R < 1 indicates a clustered vesicle distribution and R > 1 an ordered vesicle pattern; the higher the R value, the more ordered the vesicle distribution pattern
Mean glass size as outlined on vesicle wall segments	Mean glass grain size, computed from glass grain size distribution in measured image area. Glass grains are defined as glass outlined on vesicle wall segments or watershed pieces of quenched glass
Mean glass elongation as outlined on vesicle wall segments	Mean elongation of glass outlined on vesicle wall segments of intact pyroclasts, computed from glass grain shape distribution in measured thin section image. Defined as the ratio of the width and length of the outlined vesicle wall segments, comparable to grain elongation measured by dynamic image analysis
Grains from crushed and sieved pyroclasts	
Mean grain elongation	Mean elongation of glass grains from crushed pyroclasts. Defined as the ratio of the width and length of the grain, comparable to grain elongation measured by dynamic image analysis

per image was preferred over calculating average values from multiple images. For consistency, we chose to analyze both grain shapes and vesicle shapes using the same software (CSDCorrections). Since, to our knowledge, CSDCorrections has not been applied to vesicles before, duplicate measurements were performed with FOAMS, yielding vesicularities within ± 5% of the results from CSDCorrections.

Glass elongation was obtained from outlined vesicle wall segments created by the watershed function in ImageJ (Fig. 2), which separates shape outlines based on image irregularities (e.g., vesicles, thinner pieces of glass, or edges of microlites). Since the glass is most likely to break along these irregularities, crushed pyroclast grains would take similar shapes as these watershed-created outlines of vesicle wall segments.

Two images were analyzed per thin section. Mean values for vesicularity, vesicle size, glass size, and elongation as outlined on vesicle wall segments, and vesicle spatial distribution R were calculated per image (Table 3). The analyzed area of each image ranged between 5.5–75 mm^2.

From each deposit, three crushed pyroclasts that had been measured on the dynamic image analysis system were selected for analysis under the microscope. One image per pyroclast was analyzed, taken at optimal magnification levels to balance the trade-off between sufficient grain boundary resolution and the highest possible number of grains included in the image. An average number of 207 grains were measured per image. Individual grains formed by glass from broken vesicle walls were outlined and processed using ImageJ and CSDCorrections 1.6. This yielded the mean stereologically converted three-dimensional (3D) grain elongation, which we compared to the grain elongation data obtained with dynamic image analysis from the same pyroclasts. These images

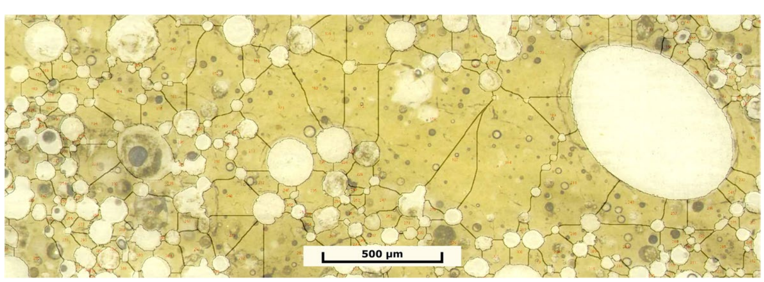

Fig. 2 Watershed interpretation of glass grain shapes (thin black lines) in thin section of intact pyroclast from the Pu'upua'i tephra cone of the Kīlauea Iki eruption (local vesicularity from image analysis: 36%)

also gave qualitative insights on the effects of grain size on shape distribution.

Results

Vesicularity distribution of data

Overall, individual pyroclast vesicularities fall between 52–98% (Fig. 3), with a peak around 95–97%, which is representative of Keanakāko'i Tephra unit B and the Halema'uma'u September 2021 and June 2023 reticulite pyroclasts. Keanakāko'i Tephra unit K1 and the Pu'upua'i tephra cone record the lowest vesicularities. The widest range of vesicularities in a single tephra deposit was recorded by Keanakāko'i Tephra unit K1 (52–92%) and the Halema'uma'u June 2023 eruption (60–96%).

Correlation between vesicularity and grain shape parameters

Mean values for the various grain shape parameters were computed for individually crushed pyroclasts and by grain size bin. All shape parameters (sphericity, elongation, compactness, and Krumbein roundness) show a negative correlation with vesicularity (Fig. 4A–D): the higher the vesicularity, the less regular the grains. Part of the scatter in the results, especially looking at Krumbein roundness (Fig. 4A) and sphericity (Fig. 4B), is due to the variety in deposits. For example, Keanakāko'i unit K1 generally shows slightly lower shape parameter values than other deposits for the same vesicularity, whereas Keanakāko'i unit K2 shows much higher Krumbein roundness values than other deposits for the same vesicularity. This effect is likely an attribute of varying vesicle textures due to varying fragmentation processes across deposits.

To quantify the degree of correlation between vesicularity and shape parameters, 1st to 8th order polynomial trendlines were fitted to the observations, showing that a maximum degree of correlation is reached by the 4th order polynomial (Fig. 5). For the complete dataset of mean vesicularity and grain shape values for individually crushed pyroclasts, the fitted 4th order polynomial trendlines yielded R^2 values of 0.57–0.76, meaning that 57% (for sphericity) to 76% (for elongation) of the variation in the observations can be explained by the fitted models (Fig. 4).

Influence of grain size on vesicularity and shape parameters

For certain grain size bins (discussed below) the correlations are more definitive (Figs. 6, 7, 8 and 9). Figure 10 shows R^2 values of the best fitting 4th order polynomial trendlines for both individual pyroclasts and data separated by grain size bins. Elongation is best correlated to vesicularity for the 88–125 μm grain size bin, compactness for the 88–125 and 125–177 μm grain size bins, sphericity for the 125–177 and 177–250 μm grain size bins, and Krumbein roundness for the 250–355 μm grain size bin. All shape parameters display a decreasing degree of correlation for both smaller and larger grain sizes.

Figure 11A shows the most dominant grain size mode (i.e., the most common grain size) in each individually crushed pyroclast (i.e., per data point in Fig. 4A–D), plotted against the vesicularity of that pyroclast from gas pycnometry. The most dominant grain size mode is calculated from dynamic image analysis data, using Blott and Pye (2001). Larger grain sizes are more common in lower vesicularity samples, whereas smaller grain sizes are more common in higher vesicularity samples. The plot also shows the general degree of grain shape regularity, calculated by adding normalized values of Krumbein roundness, sphericity, elongation, and compactness, and again normalizing the result between 0 and 1. As for

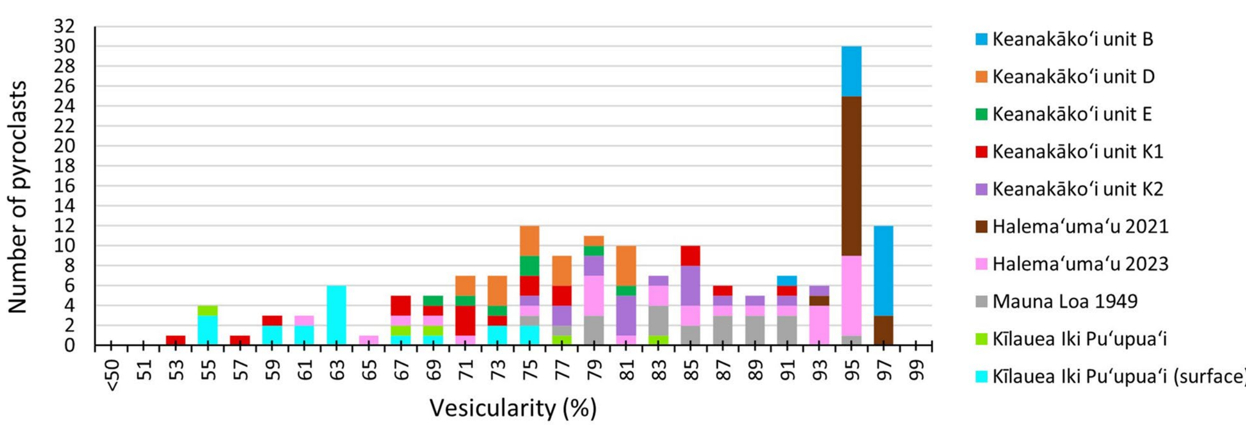

Fig. 3 Vesicularity distribution of the complete pyroclast suite, obtained via pycnometry

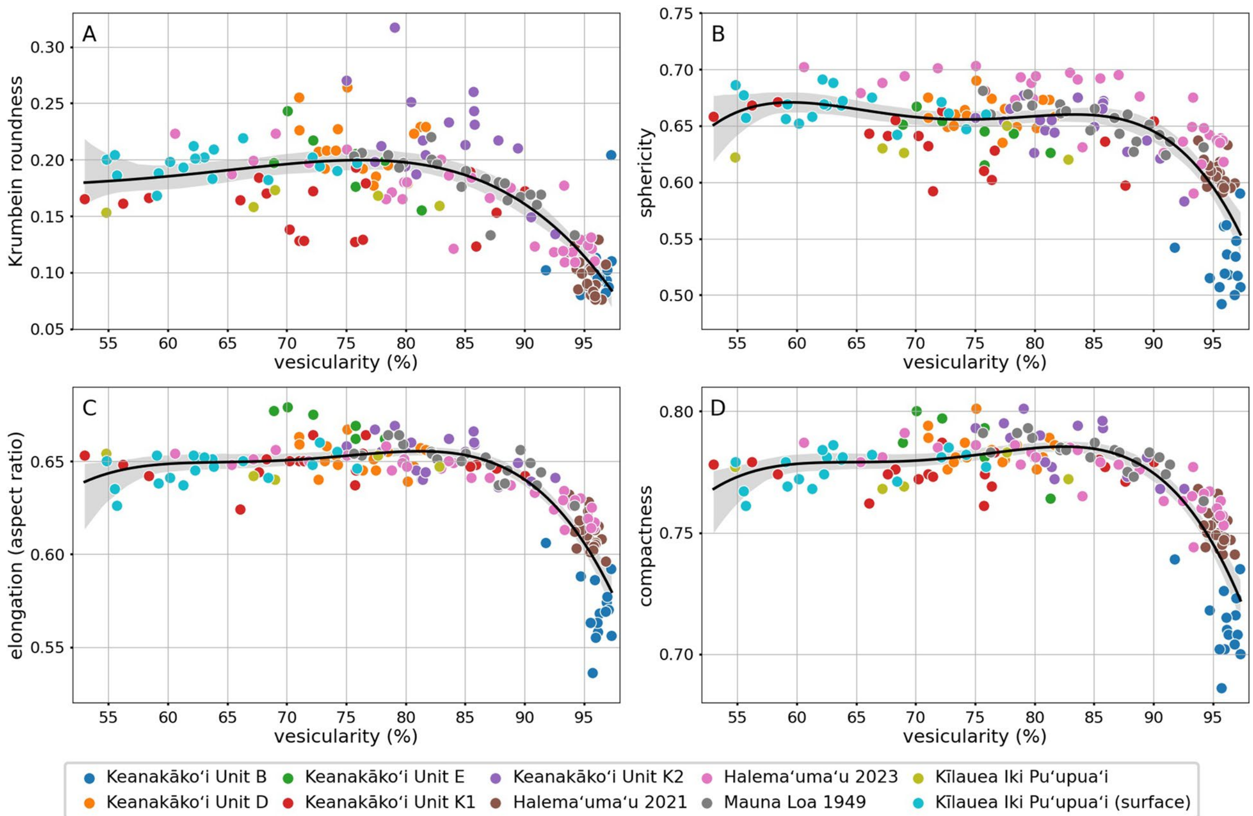

Fig. 4 Correlation between vesicularity versus mean grain shape parameters for individual pyroclasts from all sampled units for all grain sizes. Vesicularity plotted against (**A**) Krumbein roundness, (**B**) sphericity, (**C**) elongation, and (**D**) compactness, with pyroclasts plotted by tephra deposit (same colors as in Fig. 3). The solid black lines show the 4th order polynomials and corresponding 95% confidence intervals are gray shaded areas

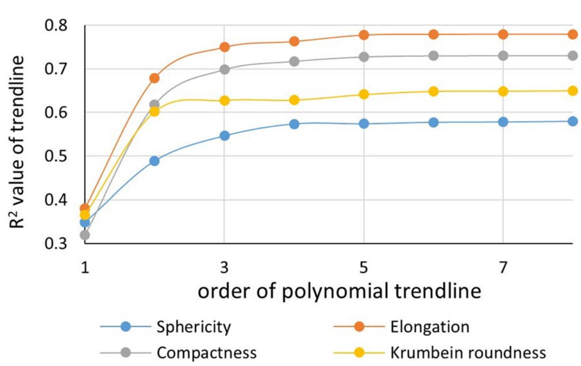

Fig. 5 R^2 values of 1st to 8th order polynomial trendlines fitted to mean vesicularity and grain shape (sphericity, elongation, compactness, and Krumbein roundness) observations for individually crushed pyroclasts

the individual shape parameters, low values represent irregular grains and high values represent more regular, smooth, and round grains. Crushed pyroclasts in which smaller grain sizes are more common show a clear decrease of shape regularity with increasing vesicularity, whereas crushed pyroclasts in which larger grain sizes are more common do not show this correlation. This supports the R^2 values shown in Fig. 10. The same relation is shown by Fig. 11B, where each crushed pyroclast is separated into grain size bins, and mean normalized shape regularity is plotted for subsets of grains within these grain size bins, against the vesicularity of its source pyroclast calculated from gas pycnometry. Note that in Fig. 11B, each pyroclast is represented by multiple data representing the different grain size bins. The figure shows that looking only at specific grain sizes, there is a relationship between grain shape and vesicularity, that is most distinct for smaller grain sizes and does not exist for grain sizes over 700 μm.

Correlation between shape parameters and grain size

All shape parameters measure different aspects of the shape of a grain. Elongation and compactness are both measurements of the area-based regularity of a grain, whereas Krumbein roundness is only influenced by irregularities in the perimeter of a grain, such as vesicle indentations. Sphericity depends on both the area

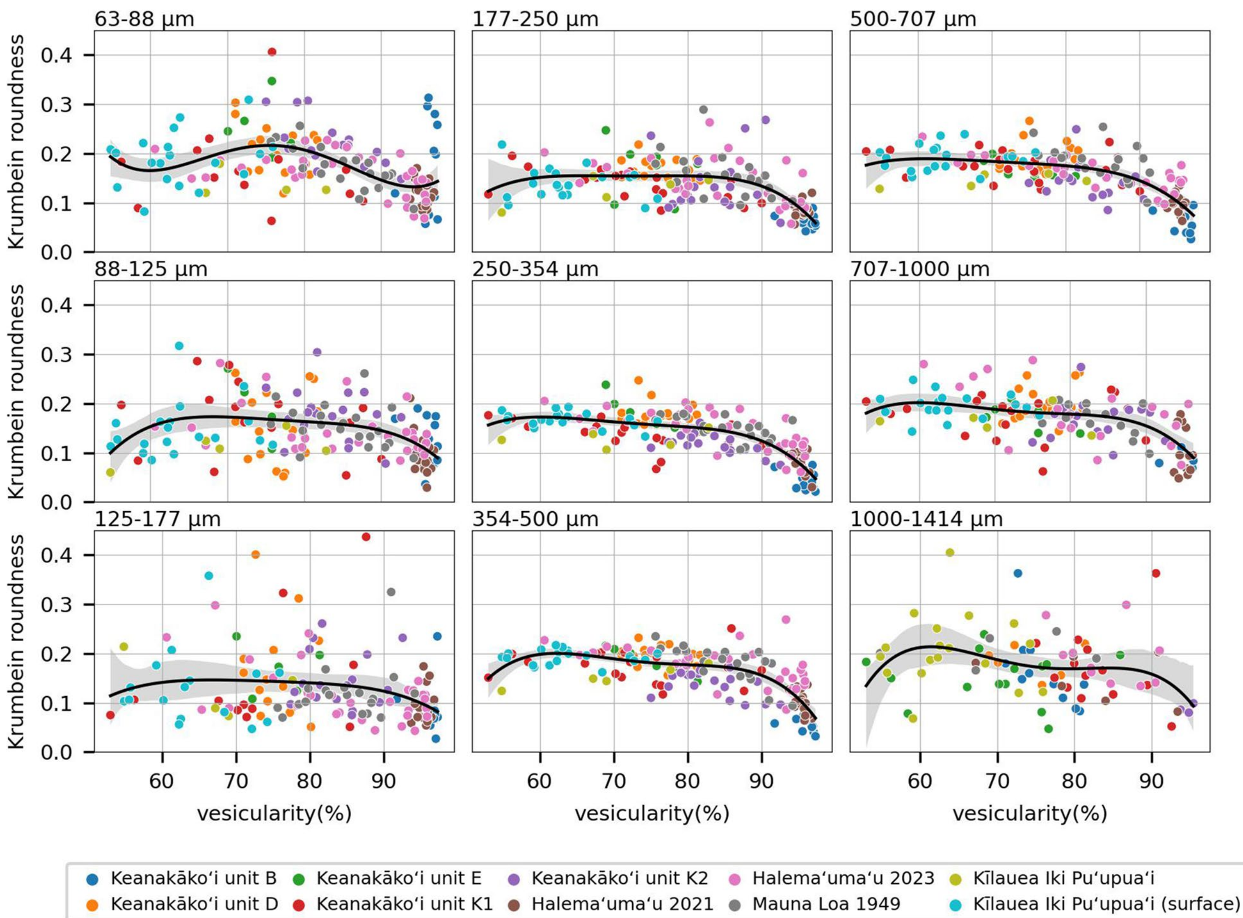

Fig. 6 Correlation between vesicularity and Krumbein roundness per grain size bin. Only data points for the grain size bin that constitutes a fraction > 1% of an entire crushed pyroclast are included

and perimeter of the grain, which is reflected in the correlations between shape parameters in our data (Fig. 12A–H), which vary with grain size and vesicularity. There is no relationship between Krumbein roundness and elongation, as these parameters are based on different aspects of shape. For small grain sizes (< 250 µm), Krumbein roundness and sphericity are not correlated, whereas sphericity shows a clear trend with elongation. For larger grain sizes (> 250 µm), Krumbein roundness and sphericity show a clear trend, whereas sphericity is not correlated to elongation. This implies that for small grains, sphericity is mostly affected by area-based irregularities, and for large grains, sphericity is mostly affected by perimeter-based irregularities. Compactness and elongation show a clear correlation for all grain sizes. Compactness decreases slightly with increasing grain size, whereas elongation increases slightly with grain size. This means larger grains are generally less elongated, but more irregular in terms of compactness. Larger grains are thus still affected by area-based shape irregularities, but more in terms of general shape distortion than elongation.

Correlation between shape parameters is greatest in grain sizes for which shape is most highly correlated with vesicularity (Figs. 10, 12A–H). The simplest explanation for this is that pyroclast shape is most strongly controlled at grain sizes approaching 250 µm, whereas outside of these particular grain size ranges, shape variations are more random. That is, for smaller grain sizes, shape distortions due to vesicles are more area-based, and for larger grain sizes they are more perimeter-based, with the tipping point at approximately 250 µm. For grains larger than 700 µm, shape is not directly related to vesicularity (Figs. 10, 11A–B).

Local effect of vesicles on pyroclast textures

Thin section images of intact pyroclasts (Fig. 13A, C, E, G, and I) show wide variations in vesicle and quenched glass textures among (1) deposits/lithologies, (2) different pyroclasts from the same deposit, or (3) even between

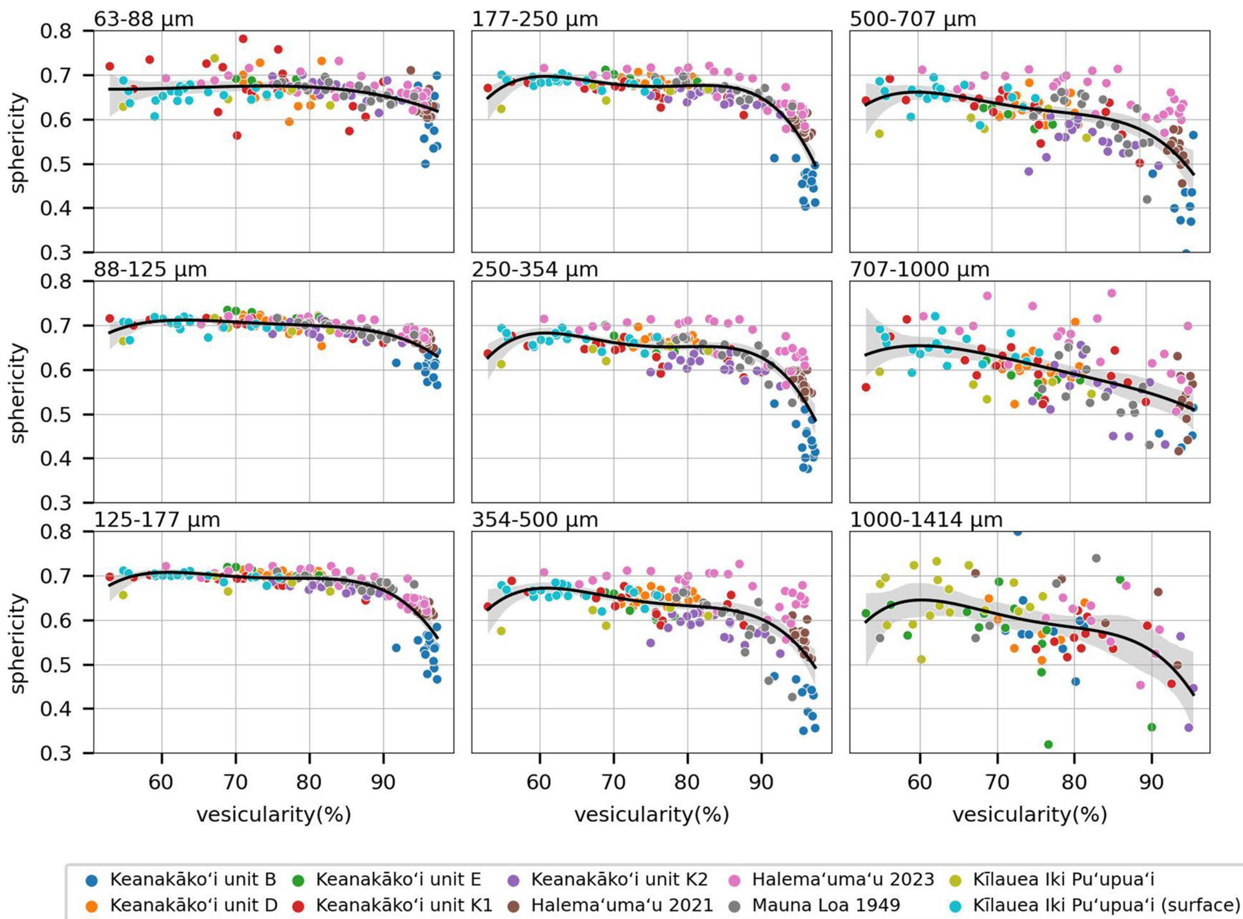

Fig. 7 Correlation between vesicularity and grain sphericity per grain size bin. Only data for the grain size bin that constitutes a fraction > 1% of an entire crushed pyroclast are included

different parts of a thin section of a given pyroclast. The structure (i.e., morphology) of interstitial glass between vesicles observed in intact pyroclasts is comparable to grain shapes crushed from pyroclasts of the same deposit (Fig. 13B, D, F, H, and J) with a similar vesicularity from the same deposit.

A selection of 15 pyroclasts crushed and analyzed by dynamic image analysis were analyzed by microscopic imaging. These analyses show that mean grain elongation values from microscopic analyses and stereological conversion differ no more than 10% from corresponding grain elongation values obtained from dynamic image analysis means (Fig. 14A–B). This technique proves to be useful in providing reliable estimates of vesicularity.

Quantitative analysis using thin section images of intact pyroclasts (Fig. 13A, C, E, G, and I) show a negative correlation between vesicularity and grain elongation (Fig. 15A-B), similar to trends from pycnometry and dynamic image analysis of grain shapes (Fig. 4C and 8). Deviations between vesicularity and grain elongation values from microscope analysis and CAMSIZER® dynamic image analysis can be explained by the differences between these methods. Notably, the microscope data were obtained from a thin section, which cuts the interstitial glass arbitrarily and may alter the grain shape, and that 2D vesicularity is known to be different from whole clast pycnometry vesicularity values (Shea et al. 2010b). Additionally, for the microscope data, each data point represents one microscope image from a small area (~ 28 mm^2) of a thin section, whereas each data point from dynamic image analysis and pycnometry represents an entire pyroclast.

The correlation between vesicularity and mean grain elongation recorded in the dynamic image analysis data can be explained by very local effects of vesicles on surrounding glass textures visible in microscope images.

Additionally, microscope images show a clear correlation between vesicularity and size ratio between vesicles and glass that was outlined on vesicle wall segments (Fig. 16A). The higher the vesicularity, the larger the

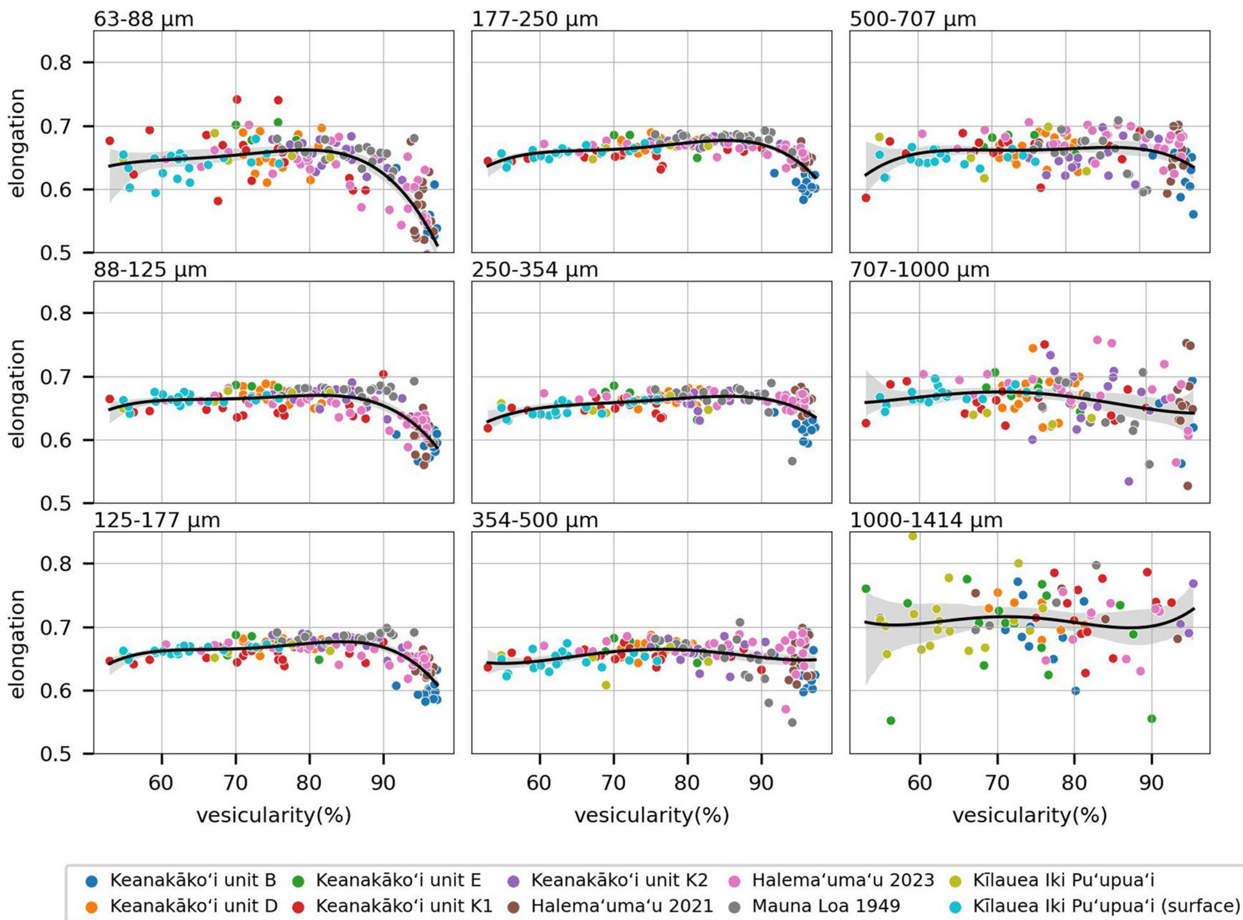

Fig. 8 Correlation between vesicularity and grain elongation per grain size bin. Only data for the grain size bin that constitutes a fraction > 1% of an entire crushed pyroclast are included

vesicles are compared to the glass outlined on vesicle wall segments between these vesicles. This supports the negative correlation between the size ratio of vesicle/glass outlined on vesicle wall segments and elongation of glass outlined on vesicle wall segments (Fig. 16B). The higher the vesicularity, the larger the vesicles and the more elongated the glass in between these vesicles.

Grain elongation is also related to vesicle spatial distribution R. If R < 1, vesicles are clustered; if R = 1, vesicles are randomly distributed; and if R > 1, vesicles are distributed in an ordered pattern. In our dataset, R generally increases with increasing vesicularity; the vesicle distribution becomes more ordered when the vesicles are larger, more abundant, and consequently more closely packed. The more closely packed the vesicles, the more elongated the glass in between the vesicles. This is consistent with the negative correlation between the elongation of glass outlined on vesicle wall segments and vesicle spatial distribution R (Fig. 16C). When vesicles are clustered (R < 1), the mean vesicle size will likely be large, but glass grains of vesicle wall segments are likely to be less elongated than in a sample where vesicles are ordered. This creates outliers on the size ratio – elongation of glass outlined on vesicle wall segment plot (Fig. 16B).

Discussion

Vesicularity limits and grain size dependency

The data show a clear correlation between vesicularity and grain shape. Higher vesicularities create more irregular glass grain shapes due to closer packing of vesicles and the resultant thinning of vesicle walls visible in microscope images (Fig. 13A–J). The shape parameter that most clearly depends on vesicularity is elongation or aspect ratio (Fig. 5). This correlation is more evident for vesicularities that range from 80 to 97% (Fig. 17).

In contrast to the data from dynamic image analysis, our microscope data show a correlation for vesicularities < 80% as well (Fig. 15A–B). The watershed interpretation of glass shapes in microscope images enabled us to restrict predicted grain sizes to the width of the solid

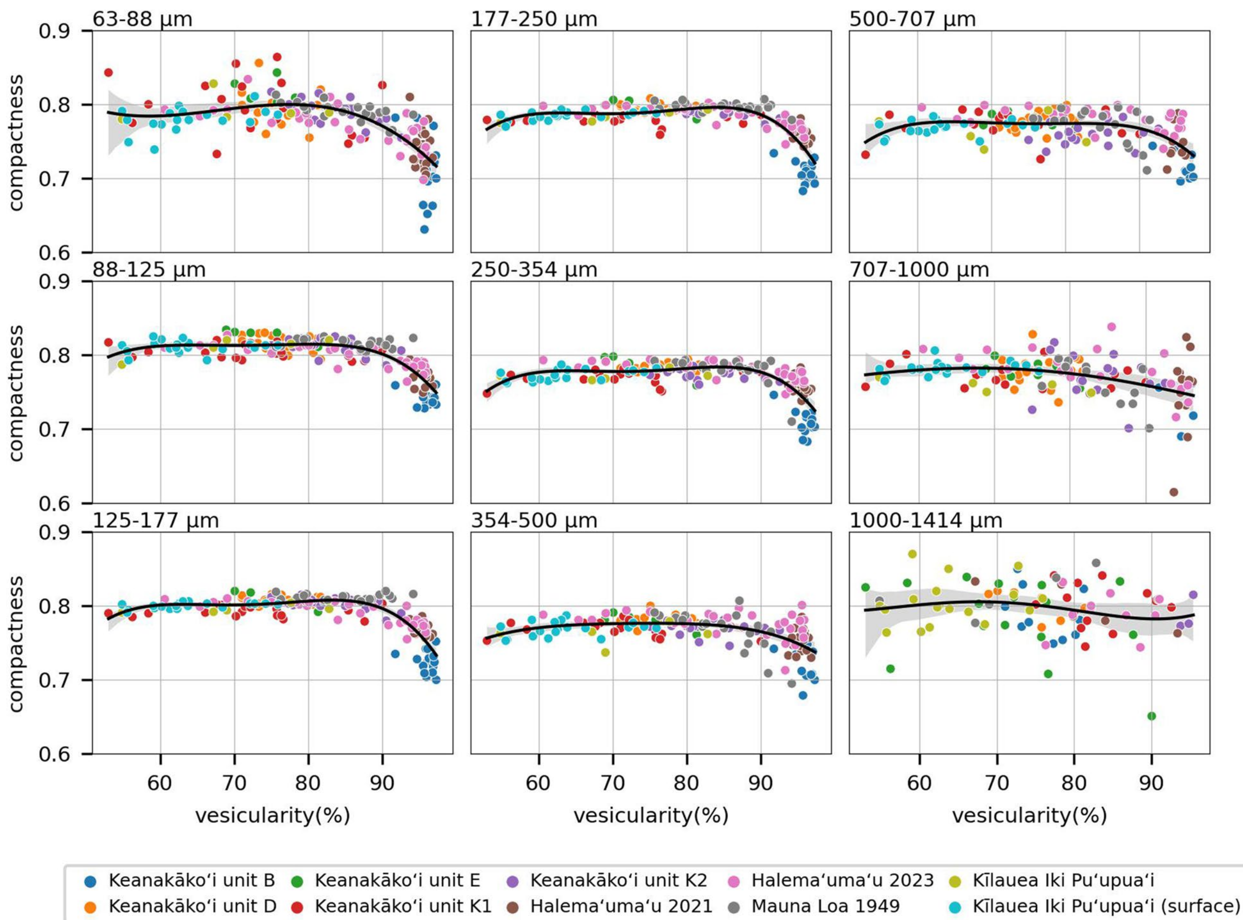

Fig. 9 Correlation between vesicularity and grain compactness per grain size bin. Only data for the grain size bin that constitutes a fraction > 1% of an entire crushed pyroclast are included

structure in between vesicles (Fig. 2). The lower the vesicularity, the wider the patches of glass in between vesicles, the larger the mean grain size and the smaller the mean vesicle size (Fig. 16A–C). As expected, the thickness of vesicle walls decreases with increasing vesicularity. Grains that are much larger than the surrounding vesicles are less affected by these vesicles than grains that are smaller than the surrounding vesicles. Decreasing vesicularity should be accompanied by increasing grain size and decreasing grain irregularity until a certain threshold is reached where vesicles have no influence on surrounding glass particle shapes anymore; however, this correlation does not consider that grain size also depends on the type of fragmentation that occurs.

Our data from dynamic image analysis show a strong grain size dependency for the degree of correlation between vesicularity and grain shapes (Figs. 6, 7, 8, 9, 10, 11A–B). This is supported by the observations of Mele and Dioguardi (2018) with a parabolic trend correlating grain irregularity with grain size. Each shape parameter in our data has an optimum grain size for which the particle shape is influenced most strongly by vesicles (Figs. 6, 7, 8 and 9), although this optimum grain size presumably varies with vesicularity and vesicle size by looking at microscope images.

Ideally, only grain shapes for grains with sizes approximately equal to the width of the solid structure in between vesicles are measured. Our data indicate that for Hawaiian basaltic tephra deposits, this ideal size range lies approximately between 60–700 µm. In the smaller size range of 60–250 µm, grain shape distortions due to vesiculation are mostly area-based, since vesicles are generally larger than grains in this size range. This causes the vesicles to create elongated grains, instead of only creating small indentations in the perimeter of the grain. These area-based shape distortions in small grains capture the influence of vesicularity on grain shape in high-vesicularity samples (Fig. 17). The reason for this is that the grain shapes that are measured in this vesicularity range are those of vesicle walls. For vesicularities between 80–97%, elongation of grains in the size range

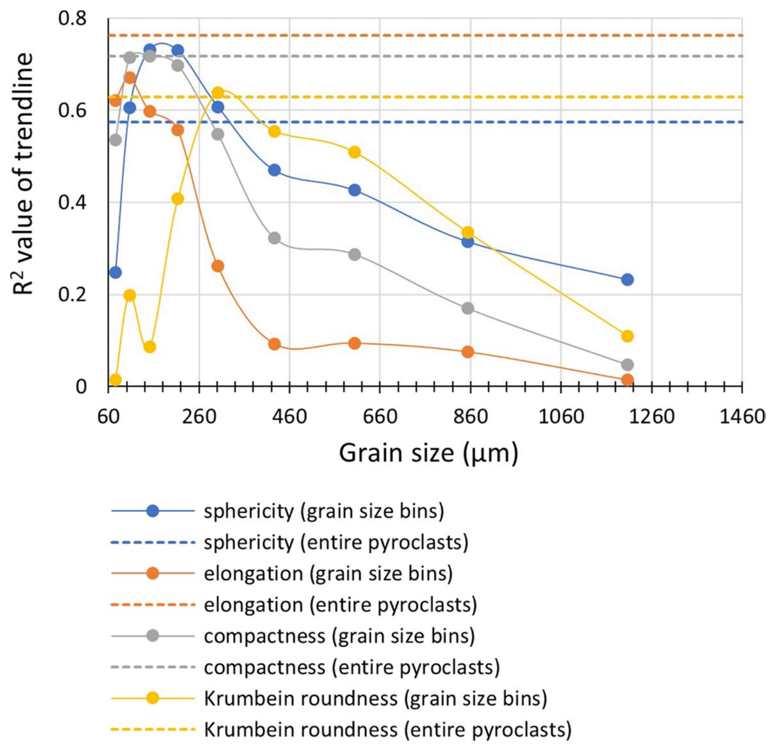

Fig. 10 Values of R^2 for the best fitting 4.th order polynomial trendlines representing the correlation between vesicularity and shape parameters, both for grain size bins (markers connected by solid lines) and for the complete dataset that includes all grain sizes for individual pyroclasts (dashed lines)

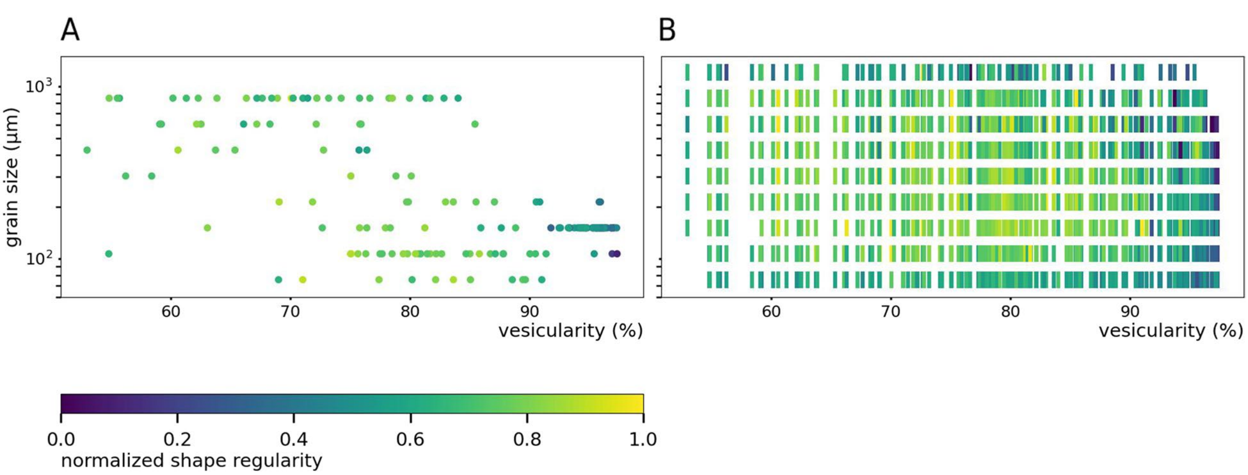

Fig. 11 The influence of grain size on the correlation between vesicularity and grain shape. Vesicularity values here represent vesicularities per pyroclast measured by pycnometry as in Fig. 4A-D. The color scale shows the general degree of shape regularity, calculated by adding up normalized values of elongation, sphericity, Krumbein roundness and compactness and normalizing the results between 0 and 1. **A** Vesicularity plotted against most dominant modal grain size of individually crushed pyroclasts. Each data point represents one crushed pyroclast sample, as in Fig. 4A-D. The most dominant modal grain size in each of these pyroclasts is calculated from dynamic image analysis data using Blott and Pye (2001). **B** Vesicularity plotted against grain size bin. Each data point (stripe) represents a subset of grains of one crushed pyroclast sample that fall in a certain grain size bin. Hence, every data point in (**A**) corresponds to multiple data in (**B**), representing one specific pyroclast

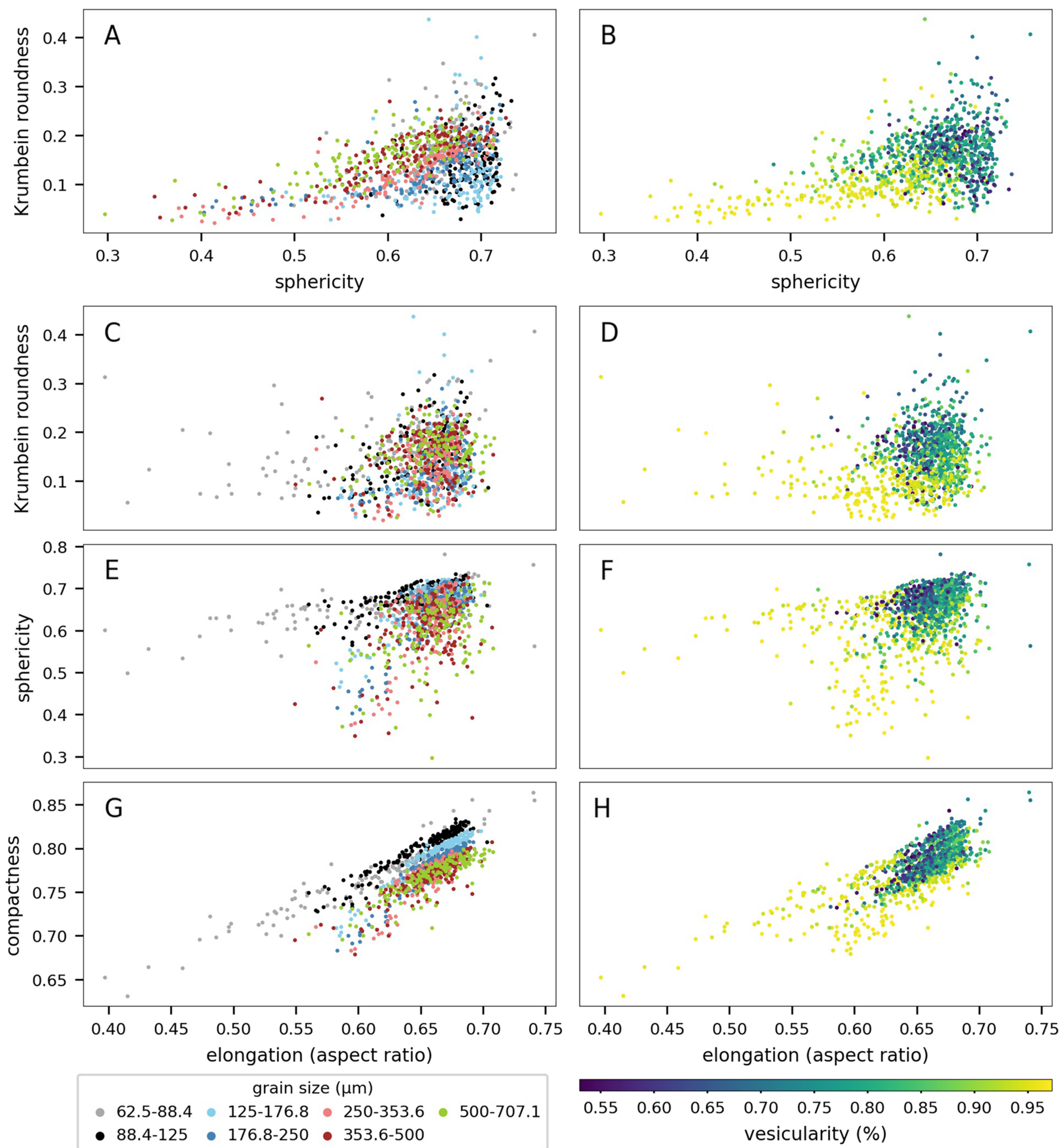

Fig. 12 Relationships between shape parameters. **A**–**B** show sphericity plotted against Krumbein roundness. The other plots show elongation plotted against Krumbein roundness (**C**–**D**), sphericity (**E**–**F**), and compactness (**G**–**H**). Colors represent grain size (left) and vesicularity (right). Each crushed pyroclast is represented by multiple data: one for each grain size bin that constitutes a fraction > 1% of the entire crushed pyroclast. Each data point shows the mean shape parameter values for grains within that particular grain size bin. Grain sizes > 700 μm are left out to enhance visibility of data, and because their shape is not correlated to vesicularity (Figs. 10 and 11)

60–250 μm is therefore a very good indicator of vesicularity (Fig. 10). In pyroclasts with lower vesicularities, the width of the solid structure in between vesicles becomes larger and measured grain shapes are not exclusively vesicle walls. In this case, the influence of vesicles is likely better captured by larger grains. In the size range 250–700 μm, grain shape distortions are more perimeter-based, meaning vesicles create small indentations in the perimeter of a grain. These shape variations are best captured by the parameter Krumbein roundness (Fig. 10), which might therefore be an interesting vesicularity indicator for vesicularities < 80%. Grains of 250–700 µm are not abundant in our data, but Krumbein roundness measurements in this size range could be explored more and might contribute to expanding the proposed method to lower vesicularities. Measuring grains in the 355–500 µm size range, Mele et al. (2018) observed increasing grain shape irregularity with increasing vesicularity for samples with lower vesicularities (5–60%). This is likely attributed to not having to deal with unevenly distributed vesicles, as their X-ray microtomography method allowed for determination of vesicularity for each individual grain, instead of for an entire pyroclast that is crushed and of which the grains are measured for shapes. In our data, even larger grain sizes of 700–1000 µm are most common in samples with vesicularities < 80%, presumably due to more difficult manual crushing for lower vesicularity samples. These larger grains may incorporate vesicles (Fig. 18) and would thus not be representative for the solid structure between vesicles, and therefore their shapes would not be directly correlated to the vesicularity of the pyroclast. A better method for crushing low vesicularity pyroclasts is needed to verify if our method works for lower vesicularities as well.

Data uncertainties and validity of results

Effect of secondary fragmentation

Pyroclasts can experience multiple phases of fragmentation, through secondary fragmentation, recycling within a lava fountain, or fracturing and abrasion within pyroclastic density currents (Houghton and Wilson 1989; Alidibirov and Dingwell 1996; Mangan and Cashman 1996; Parfitt 1998, 2004; Shea et al. 2010a, 2010b; Muller et al. 2011; Stovall et al. 2011, 2012; Alfano et al. 2012; Parcheta et al. 2013; Burgisser and Degruyter 2015; Cashman and Scheu 2015; Gonnermann 2015; Colombier et al. 2018, 2021, 2023; Figueiredo et al. 2022). The path a pyroclast is ejected within a lava fountain influences its vesiculation history. Due to thermal gradients within a lava fountain, pyroclasts transported along the margins of a lava fountain are cooled faster than those that travel through its center (Mangan and Cashman 1996; Cashman and Scheu 2015). Pyroclasts that undergo a slower cooling process yield more mature vesicle populations. In contrast, rapidly cooled pyroclasts preserve less vesicular and more fluidal textures. Post-fragmentation processes (i.e., vesiculation, shrinking) are more limited in the latter case (Stovall et al. 2011).

Only vesicles quenched rapidly after vesiculation contain information on conduit dynamics, whereas syn- and post-fragmentation vesiculation contain information on eruption dynamics. Vesicularity measurements of pyroclasts made during this study might have incorporated vesicles formed by post-fragmentation vesiculation. Of all sizes of vesicles, the ones that are in the same size range as the grains are expected to have the largest effect on the surface irregularity of those grains (Mele and Dioguardi 2018). As part of the variation in our data is presumably the result of overestimating vesicularity due to the presence of post-fragmentation vesiculation, these samples are likely to record more regular grains than expected for their estimated vesicularity.

Phenocryst and microlite content

Grain shapes and vesicle distributions are strongly influenced by the presence of microlites and phenocrysts (Schipper et al. 2010). Therefore, it is likely that the correlation between vesicularity and grain shapes found in this study only applies to pyroclasts with a relatively low phenocryst and microlite content, as are common for the relatively hot magmas of Hawaiʻi (Polacci et al. 2006; La Spina et al. 2021). This may explain why the unit E tephra from a subplinian eruption with clasts showing abundant microlites does not fit the correlation well (Figs. 4, 6–9).

Minor abundances of small olivine phenocrysts (< 1%, to < 1 mm diameter) have been observed in some hand samples and are presumably present in others. This would result in the DRE density of these samples being higher than the average 2.9 g/cm^3 used in this study, resulting

(See figure on next page.)

Fig. 13 Photomicrographs of pyroclasts from intact thin sections and crushed grains. **A** Thin section of intact pyroclast from Halemaʻumaʻu 2021 (local vesicularity from image analysis: 97%). **B** Grains of crushed and sieved pyroclast from Halemaʻumaʻu 2021 (vesicularity of entire pyroclast from pycnometry: 97%). **C** Thin section of intact pyroclast from Keanakākoʻi Tephra unit B (local vesicularity from image analysis: 90%). **D** Grains of crushed and sieved pyroclast from Keanakākoʻi Tephra unit B (vesicularity of entire pyroclast from pycnometry: 96%). **E** Thin section of intact pyroclast from Keanakākoʻi Tephra unit K2 (local vesicularity from image analysis: 80%). **F** Grains of crushed and sieved pyroclast from Keanakākoʻi Tephra unit K2 (vesicularity of entire pyroclast from pycnometry: 84%). **G** Thin section of intact pyroclast from Kīlauea Iki tephra from Puʻupuaʻi (local vesicularity from image analysis: 60%). **H** Grains of crushed and sieved pyroclast from Kīlauea Iki tephra from Puʻupuaʻi (vesicularity of entire pyroclast from pycnometry: 67%). **I** Thin section of intact pyroclast from Keanakākoʻi Tephra unit E (local vesicularity from image analysis: 30%). **J** Grains of crushed and sieved pyroclast from Keanakākoʻi Tephra unit E (vesicularity of entire pyroclast from pycnometry: 69%)

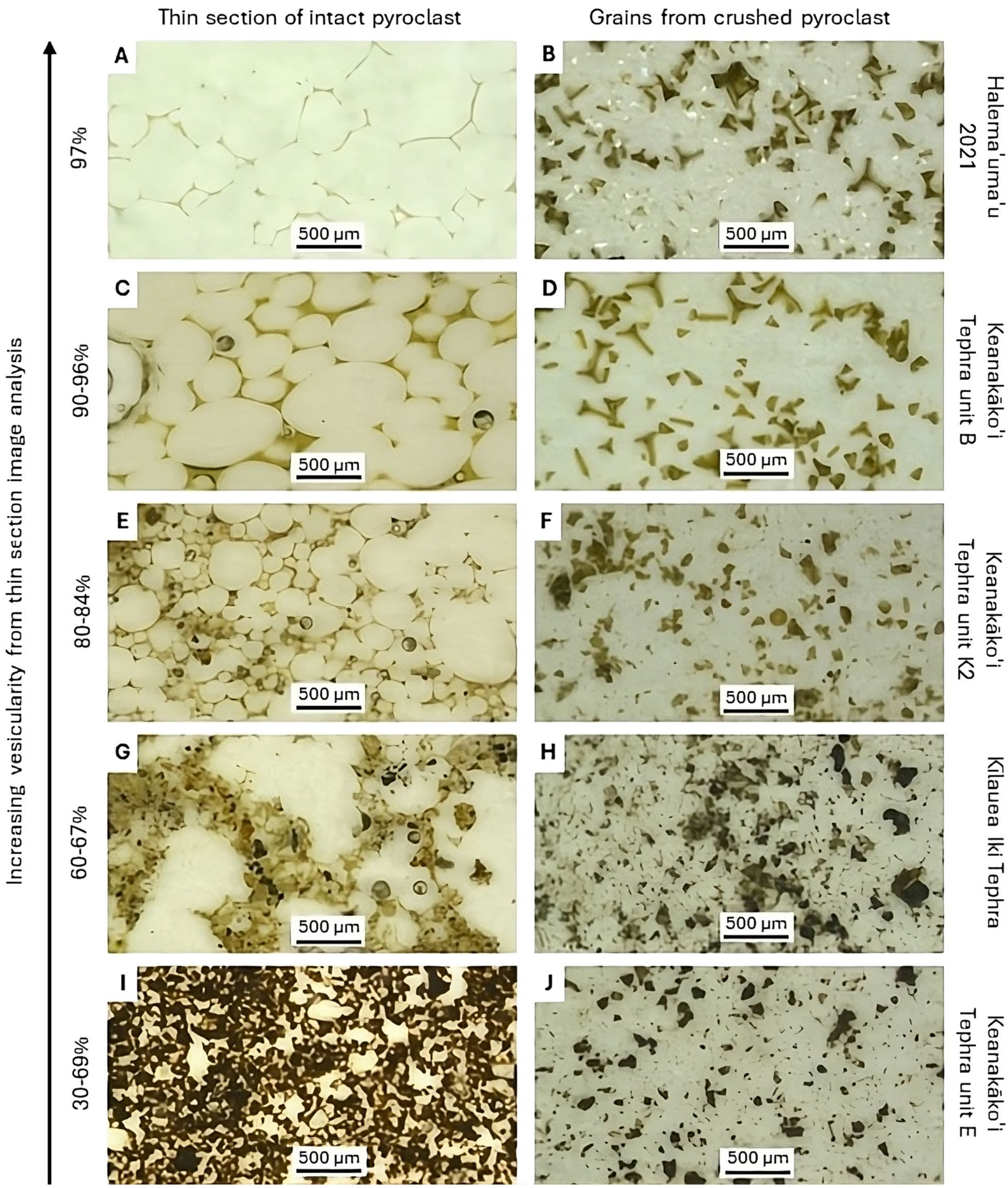

Fig. 13 (See legend on previous page.)

in a slight underestimation of vesicularities. However, the small volumes of these phenocrysts and microlites are deemed negligible.

Conclusions

Our data show a clear correlation between vesicularity and grain morphology for pyroclasts from multiple

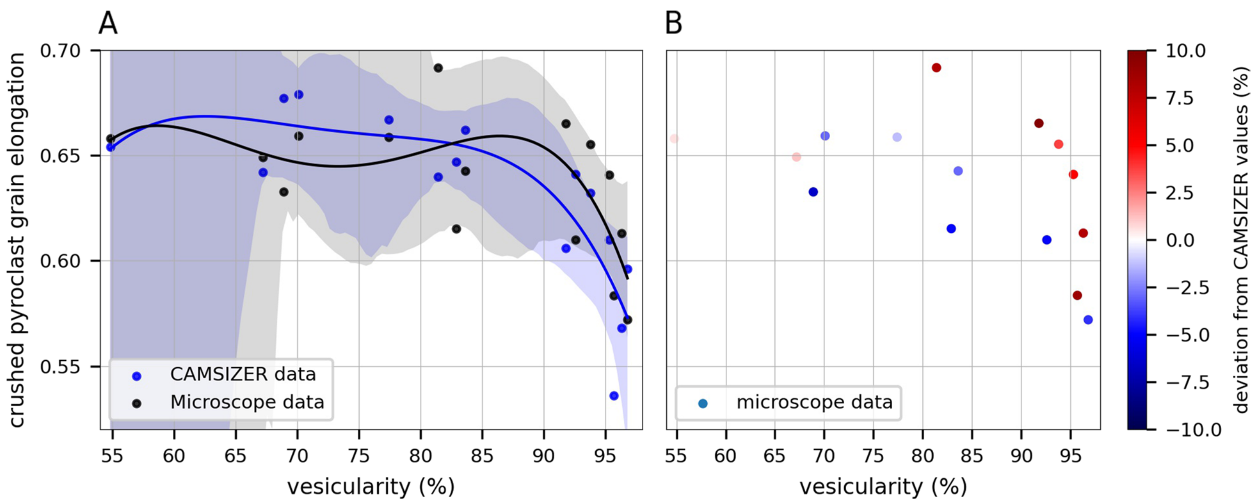

Fig. 14 Comparison of grain elongation data from microscope image analysis with stereological conversion and dynamic image analysis. Each data point represents one crushed pyroclast. An average number of 207 grains was measured per microscope image. **A** Grain elongation from microscope analysis (black) and grain elongation from dynamic image analysis (blue) for the same pyroclasts plotted against entire pyroclast vesicularity from pycnometry. Trendlines of the 4th order polynomials are shown with 95% confidence intervals (shaded areas). **B** Grain elongation from microscope analysis plotted against entire pyroclast vesicularity from pycnometry, with color ramp showing the percent deviation from the corresponding grain elongation values measured by dynamic image analysis

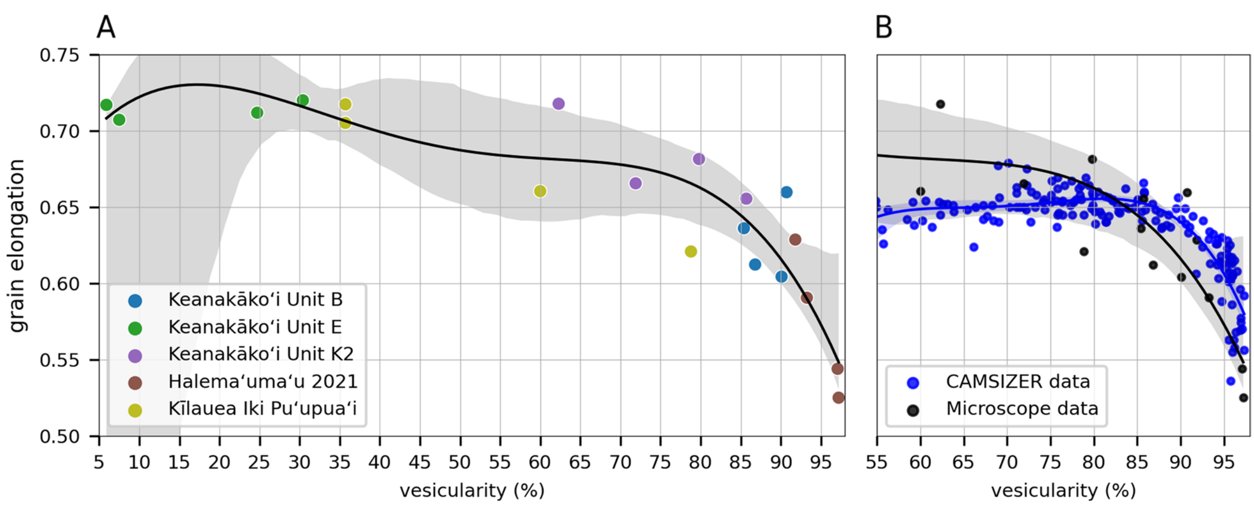

Fig. 15 **A** Correlation between local vesicularity and elongation of glass outlined on vesicle wall segments from microscope images, categorized by individual tephra deposit. Here, grain elongation values are based on watershed-created glass grain outlines from thin section images of intact pyroclasts. Vesicularity is defined as the volume areal percentage not occupied by grains of free space within clast boundaries, obtained by stereological conversion of the area of the image occupied by grain outlines. Each data point represents the mean value for one microscope image, with an average measured area of ~ 28 mm^2, showing the local influence of vesicles on glass textures. **B** Comparison of dynamic image analysis (crushed pyroclast grain elongation from dynamic image analysis and vesicularity from pycnometry) and microscope data (local elongation and vesicularity of glass outlined on vesicle wall segments from thin section image analysis and stereological conversion). Trendlines of 4.th order polynomials are shown with 95% confidence intervals (shaded areas)

tephra deposits at Hawaiian volcanoes. Grain shapes become increasingly irregular with increasing vesicularity. Here we propose dynamic image analysis on 2D projection shapes of grains from crushed pyroclasts using a dynamic image analysis system (CAMSIZER®) as a new method to estimate vesicularity of pyroclasts in near-real-time. Of all shape parameters measured by dynamic image analysis, grain elongation is most clearly correlated to vesicularity. The best fitted model, a 4th order polynomial trendline to the vesicularity and grain

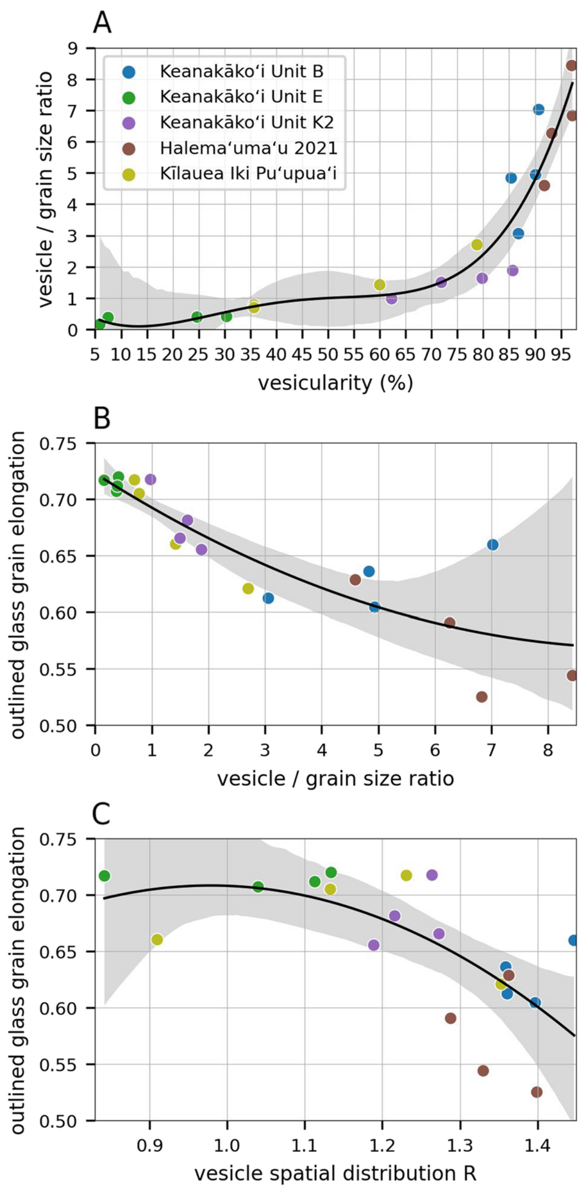

Fig. 16 Correlations between (**A**) size ratio of vesicle/glass outlined on vesicle wall segments and vesicularity, (**B**) elongation of glass outlined on vesicle wall segments and the size ratio of vesicle/glass outlined on vesicle wall segments, and (C) elongation of glass outlined on vesicle wall segments and vesicle spatial distribution R. Each data point represents the mean values for one microscope image with an average area of ~ 28 mm^2. Trendlines of 4.th order polynomials are shown with 95% confidence intervals (shaded areas)

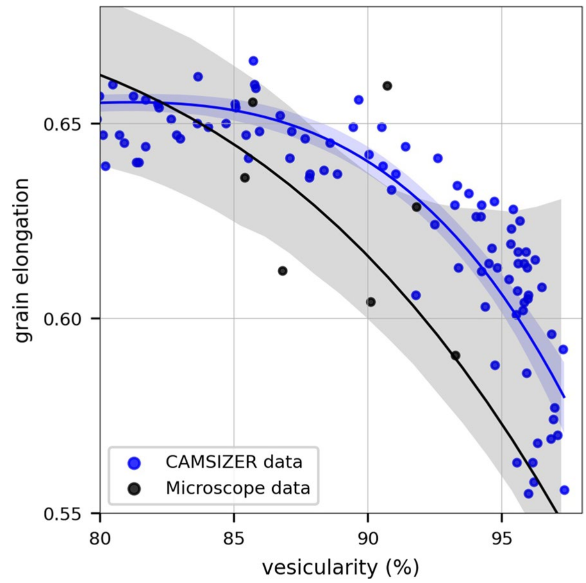

Fig. 17 Grain elongation plotted against vesicularity from both dynamic image analysis and microscope analysis (same as Fig. 15B), for vesicularities of 80–97%. The correlation is illustrated by trendlines (solid lines) and corresponding 95% confidence intervals

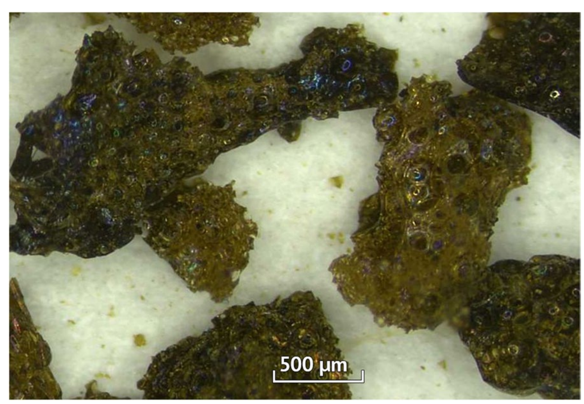

Fig. 18 Large grains (700–1000 μm) from the Pu'upua'i tephra cone of the Kīlauea Iki eruption. The grains incorporate vesicles, so their shapes do not directly reflect the vesicularity of the source pyroclast

elongation observations, explained 76% of the variation in the observations. This is roughly within the accuracy limits of eruption response analyses.

Microscope image analysis shows that the observed correlation between mean grain shape and vesicularity of entire pyroclasts can be explained by the very local (μm-scale) influence of vesicles on the shape of the solid structure in between those vesicles. Even though grain shape depends on many factors other than vesicularity, such as vesicle size and shape, vesicle number density, vesicle spatial distribution, and pyroclast grain size, the correlation between grain shape and vesicularity is clear enough to get a rough estimate of vesicularity from grain shape measurements.

Grain size has a significant influence on the correlation between vesicularity and grain shape and should be considered when using our method. Shape variation due to vesicularity in grains of 50–250 µm is best captured by the area-based shape parameter grain elongation, whereas shape variation in grains of 250–700 µm is best captured by the perimeter-based shape parameter Krumbein roundness. The latter is a better vesicularity indicator for pyroclasts with vesicularities < 80%, since these have wider vesicle walls in between vesicles, making larger grains better indicators for the influence of vesicles on grain shape. Shapes of grains larger than 700 µm are not directly related to vesicularity.

This new method to quickly gauge vesicularity can be used during eruption responses, but so far has only been successfully tested on highly vesicular (> 80%) basaltic pyroclasts with a low microlite and/or phenocryst content. It might be possible to extend the method to lower vesicularities, if low vesicularity pyroclasts can be crushed to grain sizes of less than 700 µm and grain shape measurements can be restricted to grain sizes approximately equal to the width of the solid structure between vesicles. This new method demonstrating the link between vesicularity, grain shape, and size may reveal important information on the eruptive styles of future activity at Hawaiian volcanoes.

Acknowledgements
Thoughtful reviews by Heather Wright, Fabrizio Alfano, and Mathieu Colombier, and editorial handling by Daniel Bertin, are greatly appreciated. The equipment purchases were supported by the Additional Supplemental Appropriations for Disaster Relief Act of 2019 (P.L. 116-20) following the 2018 eruption of Kīlauea volcano. Any use of trade, product, or firm names is for descriptive purposes only and does not imply endorsement by the U.S. Government.

Authors' contributions
J.S., D.T.D., and K.M.v.H. conceived the project. K.M.v.H. led the sample preparation and quantitative analysis. K.M.v.H led the writing effort and figure drafting. All authors reviewed the manuscript.

Funding
Research was funded through the U.S. Geological Survey Volcano Science Center. The Hendrik Mullerfonds and Stichting Molengraaff Fonds granted financial support to enable K.M.v.H. to perform a research internship with the U.S. Geological Survey Hawaiian Volcano Observatory as part of her master's degree at Utrecht University.

Availability of data and materials
Data are available as a U.S. Geological Survey data release by van Helden et al. (2024).

Declarations

Competing interests
The authors declare no competing interests.

Author details
[1]Department of Earth Sciences, Utrecht University, Utrecht, Netherlands. [2]U.S. Geological Survey, Hawaiian Volcano Observatory, Hilo, HI 96720, USA.

Received: 9 February 2024 Accepted: 11 July 2024
Published online: 20 July 2024

References

Alfano F, Bonadonna C, Gurioli L (2012) Insights into eruption dynamics from textural analysis: the case of the May, 2008. Chaitén eruption. Bull Volcanol. 74:2095–2108. https://doi.org/10.1007/s00445-012-0648-3
Alidibirov M, Dingwell DB (1996) Magma fragmentation by rapid decompression. Nature 380:146–148
Baker DR, Brun F, O'shaughnessy C, Mancini L, Fife JL, Rivers M (2012) A four-dimensional X-ray tomographic microscopy study of bubble growth in basaltic foam. Nature Comm 3:1135. https://doi.org/10.1038/ncomms2134
Biass S, Swanson DA, Houghton BF (2018) New perspective on the nineteenth-century golden pumice deposit of Kīlauea Volcano. In: Poland MP, Garcia MO, Camp VE, Grunder A (eds) Field Volcanology: A Tribute to the Distinguished Career of Don Swanson. Geol Soc Am Special Pap 538:227–246. https://doi.org/10.1130/2018.2538
Blott SJ, Pye K (2001) GRADISTAT: a grain size distribution and statistics package for the analysis of unconsolidated sediments. Earth Surf Process Landf 26:1237–1248. https://doi.org/10.1002/esp.261
Buckland HM, Saxby J, Roche M, Meredith P, Rust AC, Cashman KV, Engwell SL (2021) Measuring the size of non-spherical particles and the implications for grain size analysis in volcanology. J Volcanol Geotherm Res 415:107257. https://doi.org/10.1016/j.jvolgeores.2021.107257
Burgisser A, Degruyter W (2015) Chapter 11 - Magma Ascent and Degassing at Shallow Levels. In: Sigurdsson H (ed) The Encyclopedia of Volcanoes. Academic Press, Amsterdam, pp 225–236
Cáceres F, Wadsworth FB, Scheu B, Colombier M, Madonna C, Cimarelli C, Hess K-U, Kaliwoda M, Ruthensteiner B, Dingwell DB (2020) Can nanolites enhance eruption explosivity? Geology 48:997–1001. https://doi.org/10.1130/G47317.1
Cashman KV, Scheu B (2015) Chapter 25 - Magmatic Fragmentation. In: Sigurdsson H (ed) The Encyclopedia of Volcanoes. Academic Press, Amsterdam, pp 459–471
Colombier M, Wadsworth FB, Gurioli L, Scheu B, Kueppers U, Muri AD, Dingwell DB (2017a) The evolution of pore connectivity in volcanic rocks. Earth Planet Sci Lett 462:99–109. https://doi.org/10.1016/j.espl.2017.01.011
Colombier M, Gurioli L, Druitt TH, Shea T, Boivin P, Miallier D, Cluzel N (2017b) Textural evolution of magma during the 9.4-ka trachytic explosive eruption at Kilian volcano, Chaîne des Puys. France. Bull Volcanol 97:17. https://doi.org/10.1007/s00445-017-1099-7
Colombier M, Scheu B, Wadsworth FB, Cronin S, Vasseur J, Dobson KJ, Hess K-U, Tost M, Yilmaz TI, Cimarelli C, Brenna M, Ruthensteiner B, Dingwell DB (2018) Vesiculation and quenching during Surtseyan eruptions at Hunga Tonga-Hunga Ha'apai volcano, Tonga. J Geophys Res 123:3762–3779. https://doi.org/10.1029/2017JB015357
Colombier M, Wadsworth FB, Scheu B, Vasseur J, Dobson KJ, Cáceres F, Allabar A, Marone F, Schlepütz CM, Dingwell DB (2020) In situ observation of the percolation threshold in multiphase magma analogues. Bull Volcanol 82:1–15. https://doi.org/10.1007/s00445-020-1370-1
Colombier M, Vasseur J, Houghton BF, Cáceres F, Scheu B, Kueppers U, Thivet S, Gurioli L, Montanaro C, Soldati A, Muro AD, Dingwell DB (2021) Degassing and gas percolation in basaltic magmas. Earth Planet Sci Lett 573:117134. https://doi.org/10.1016/j.epsl.2021.117134
Colombier M, Manga M, Wright H, Bernard B, deGraffenried R, Cáceres F, Samaniego P, Vasseur J, Jakata K, Cook P, Dingwell DB (2023) Pre-eruptive outgassing and pressurization, and post-fragmentation bubble nucleation, recorded by vesicles in breadcrust bombs from vulcanian activity at Guagua Pichincha volcano, Ecuador. J Geophys Res 128:e2023JB026775
Figueiredo CA, Bongiolo EM, Jutzeler M, Gomes OFM, Neumann R (2022) Alkalic pyroclast morphology informs on fragmentation mechanisms, Trindade Island. Brazil J Volcanol Geotherm Res 428:107575. https://doi.org/10.1016/j.jvolgeores.2022.107575
Garcia MO, Mucek AE, Lynn KJ, Swanson DA, Norman MD (2018) Geochemical evolution of Keanakāko'i Tephra, Kīlauea volcano, Hawai'i. In: Poland MP, Garcia MO, Camp VE, Grunder A (eds). Field Volcanology: A Tribute

to the Distinguished Career of Don Swanson. Geol Soc Am Special Pap 538:203–225
Gonnermann HM (2015) Magma fragmentation. Annu Rev Earth Planet Sci 43:431–458. https://doi.org/10.1146/annurev-earth-060614-105206
Guimarães LF, Hornby A, Kueppers U, Alves A, Janasi VA, Dingwell DB (2019) Generation of block-and-ash flows at the onset of silicic volcanism in the Paraná Magmatic Province (Brazil): evidence from photoanalysis of Caxias do Sul breccias. Bull Volcanol 81:65. https://doi.org/10.1007/s00445-019-1332-7
Heiken G (1972) Morphology and petrography of volcanic ashes. Geol Soc Am Bull 83:1961–1988. https://doi.org/10.1130/0016-7606(1972)83[1961:MAPOVA]2.0.CO;2
Higgins MD (2000) Measurement of crystal size distributions. Am Mineral 85:1105–1116. https://doi.org/10.2138/am-2000-8-901
Higgins MD (2002) Closure in crystal size distributions (CSD), verification of CSD calculations, and the significance of CSD fans. Am Mineral 87:171–175. https://doi.org/10.2138/am-2002-0118
Houghton BF, Wilson CJN (1989) A vesicularity index for pyroclastic deposits. Bull Volcanol 51:451–462. https://doi.org/10.1007/BF01078811
Jerram DA, Cheadle MJ, Hunter RH, Elliott MT (1996) The spatial distribution of grains and crystals in rocks. Contrib Mineral Petrol 125:60–74. https://doi.org/10.1007/s004100050206
Krumbein WC (1941) Measurement and geological significance of shape and roundness of sedimentary particles. J Sediment Res 11:64–72. https://doi.org/10.1306/D42690F3-2B26-11D7-8648000102C1865D
La Spina G, Arzilli F, Llewellin EW, Burton MR, Clarke AB, Vitturi MM, Polacci M, Hartley ME, Genova DD, Mader HM (2021) Explosivity of basaltic lava fountains is controlled by magma rheology, ascent rate and outgassing. Earth Planet Sci Lett 553:116658. https://doi.org/10.1016/j.epsl.2020.116658
Liu EJ, Cashman KV, Rust AC (2015) Optimising shape analysis to quantify volcanic ash morphology. J Geo Res 8:14–30. https://doi.org/10.1016/j.grj.2015.09.001
Lo Castro D (2009) Andronico D (2009) Grain size distributions of volcanic particles by CAMSIZER. Conferenza Rittmann, Nicolosi (Ct), Italy, pp 11–13
Lo Castro MD, Andronico D, Nunnari G, Spata A, Torrisi A (2009) Shape measurements of volcanic particles by CAMSIZER (https://www.earth-prints.org/bitstream/2122/5617/1/LoCastro%26al_2009pdf.pdf)
Macdonald GA, Orr JB (1950) The 1949 Summit Eruption of Mauna Loa, Hawaii. U.S. Geol Sruv Bull 974-A:31. https://doi.org/10.3133/b974A
Mangan MT, Cashman KV (1996) The structure of basaltic scoria and reticulite and inferences for vesiculation, foam formation, and fragmentation in lava fountains. J Volcanol Geotherm Res 73:1–18. https://doi.org/10.1016/0377-0273(96)00018-2
Mastin LG, Guffanti M, Servranckx R, Webley P, Barsotti S, Dean K, Durant A, Ewert JW, Neri A, Rose WI, Schneider D, Siebert L, Stunder B, Swanson G, Tupper A, Volentik A, Waythomas CF (2009) A multidisciplinary effort to assign realistic source parameters to models of volcanic ash-cloud transport and dispersion during eruptions. J Volcanol Geotherm Res 186:10–21. https://doi.org/10.1016/j.jvolgeores.2009.01.008
May M, Carey RJ, Swanson DA, Houghton BF (2015) Reticulite-producing fountains from ring fractures in Kīlauea Caldera ca. 1500 CE, In: Carey R, Cayol V, Poland M, Weis D (eds). Hawaiian Volcanoes: From Source to Surface. 351–367, https://doi.org/10.1002/9781118872079.ch16.
Mele D, Dioguardi F (2018) The grain size dependency of vesicular particle shapes strongly affects the drag of particles. First results from microtomography investigations of Campi Flegrei fallout deposits. J Volcanol Geotherm Res 353:18–24. https://doi.org/10.1016/j.jvolgeores.2018.01.023
Mele D, Dioguardi F, Dellino P (2018) study on the influence of internal structures on the shape of pyroclastic particles by X-ray microtomography investigations. Ann Geophys 61:VO670. https://doi.org/10.4401/ag-7868
Mueller S, Scheu B, Kueppers U, Spieler O, Richard D, Dingwell DB (2011) The porosity of pyroclasts as an indicator of volcanic explosivity. J Volcanol Geotherm Res 203:168–174. https://doi.org/10.1016/j.jvolgeores.2011.04.006
Murtagh RM, White JDL (2013) Pyroclast characteristics of a subaqueous to emergent Surtseyan eruption, Black Point volcano, California. J Volcanol Geotherm Res 267:75–91. https://doi.org/10.1016/j.jvolgeores.2013.08.015
Namiki A, Tanaka Y, Yokoyama T (2018) Physical characteristics of scoriae and ash from 2014–2015 eruption of Aso Volcano, Japan. Earth Planets Space 70:1–21. https://doi.org/10.1186/s40623-018-0914-5
Oppenheimer J, Capponi A, Cashman KV, Lane SJ, Rust AC, James MR (2020) Analogue experiments on the rise of large bubbles through a solids-rich suspen-sion: a "weak plug" model for Strombolian eruptions. Earth Planet Sci Lett 531:115931. https://doi.org/10.1016/j.epsl.2019.115931
Parcheta CE, Houghton BF, Swanson DA (2013) Contrasting patterns of vesiculation in low, intermediate, and high Hawaiian fountains: a case study of the 1969 Mauna Ulu eruption. J Volcanol Geotherm Res 255:79–89. https://doi.org/10.1016/j.jvolgeores.2013.01.016
Parfitt EA (1998) A study of clast size distribution, ash deposition and fragmentation in a Hawaiian-style volcanic eruption. J Volcanol Geotherm Res 84:197–208. https://doi.org/10.1016/S0377-0273(98)00042-0
Parfitt EA, Wilson L (1999) A Plinian treatment of fallout from Hawaiian lava fountains. J Volcanol Geotherm Res 88:67–75. https://doi.org/10.1016/S0377-0273(98)00103-6
Parfitt EA (2004) A discussion of the mechanisms of explosive basaltic eruptions. J Volcanol Geotherm Res 134:77–107. https://doi.org/10.1016/j.jvolgeores.2004.01.002
Pisello A, Kueppers U, Düffels K, Nomikou P, Dingwell DB, Perugini D (2023) The porosity of felsic pyroclasts: laboratory validation of field-based approaches. Bull Volcanol 85:69. https://doi.org/10.1007/s00445-023-01679-4
Polacci M, Corsaro RA, Andronico D (2006) Coupled textural and compositional characterization of basaltic scoria: insights into the transition from Strombolian to fire fountain activity at Mount Etna, Italy. Geology 34:201–204. https://doi.org/10.1130/G22318.1
Pyle D (1989) The thickness, volume and grainsize of tephra fall deposits. Bull Volcanol 51:1–15. https://doi.org/10.1007/BF01086757
Richter DH, Eaton JP, Murata KJ, Ault WU, Krivoy HL (1970) Chronological narrative of the 1959–60 eruption of Kilauea Volcano, Hawaii. US Geol Surv Prof Pap 573-E:73. https://doi.org/10.3133/pp537E
Ross P-S, Dürig T, Comida PP, Lefebvre N, White JDL, Andronico D, Thivet S, Eychenne J, Gurioli L (2022) Standardized analysis of juvenile pyroclasts in comparative studies of primary magma fragmentation; 1. Overview and Workflow Bull Volcanol 84:13. https://doi.org/10.1007/s00445-021-01516-6
Rust AC, Cashman KV (2011) Permeability controls on expansion and size distributions of pyroclasts. J Geophys Res 116:B11202. https://doi.org/10.1029/2011JB008494
Sahagian DL, Proussevitch AA (1998) 3D particle size distributions from 2D observations: stereology for natural applications. J Volcanol Geotherm Res 84:173–196. https://doi.org/10.1016/S0377-0273(98)00043-2
Saxby J, Beckett F, Cashman K, Rust A, Tennant E (2018) The impact of particle shape on fall velocity: implications for volcanic ash dispersion modelling. J Volcanol Geotherm Res 362:32–48. https://doi.org/10.1016/j.jvolgeores.2018.08.006
Schipper CI, White JDL, Houghton BF (2010) Syn- and post-fragmentation textures in submarine pyroclasts from Lō`ihi Seamount, Hawai`i. J Volcanol Geotherm Res 191:93–106. https://doi.org/10.1016/j.jvolgeores.2010.01.002
Schmith J, Höskuldsson Á, Holm PM (2017) Grain shape of basaltic ash populations: implications for fragmentation. Bull Volcanol 79:14. https://doi.org/10.1007/s00445-016-1093-5
Schmith J, Swanson DA (2023) Complex styles of phreatomagmatic explosions at Kīlauea Volcano, Hawaii, controlled by magma structure. Front Earth Sci 11:1153288. https://doi.org/10.3389/feart.2023.1153288
Schneider CA, Rasband WS, Eliceiri KW (2012) NIH Image to ImageJ: 25 years of image analysis. Nat Methods 9:671–675. https://doi.org/10.1038/nmeth.2089
Self S, Sparks RSJ (1978) Characteristics of widespread pyroclastic deposits formed by the interaction of silicic magma and water. Bull Volcanol 41:196–212. https://doi.org/10.1007/BF02597223
Sharp RP, Dzurisin D, Malin MC (1987) An early 19th century reticulite pumice from Kilauea volcano. US Geol Surv Prof Pap 1350:395–404
Shea T, Houghton BF, Gurioli L, Cashman KV, Hammer JE, Hobden BJ (2010a) Textural studies of vesicles in volcanic rocks: an integrated methodology. J Volcanol Geotherm Res 190:271–289. https://doi.org/10.1016/j.jvolgeores.2009.12.003

Shea T, Gurioli L, Larsen JF, Houghton BF, Hammer JE, Cashman KV (2010b) Linking experimental and natural vesicle textures in Vesuvius 79AD white pumice. J Volcanol Geotherm Res 192:69–84. https://doi.org/10.1016/j.jvolgeores.2010.02.013
Stovall WK, Houghton BF, Gonnermann H, Fagents SA, Swanson DA (2011) Eruption dynamics of Hawaiian-style fountains: the case study of episode 1 of the Kīlauea Iki 1959 eruption. Bull Volcanol 73:511–529. https://doi.org/10.1007/s00445-010-0426-z
Stovall WK, Houghton BF, Hammer JE, Fagents SA, Swanson DA (2012) Vesiculation of high fountaining Hawaiian eruptions: episodes 15 and 16 of 1959 Kīlauea Iki. Bull Volcanol 74:441–455. https://doi.org/10.1007/s00445-011-0531-7
Swanson DA, Rose TR, Fiske RS, McGeehin JP (2012) Keanakākoʻi Tephra produced by 300 years of explosive eruptions following collapse of Kīlauea's caldera in about 1500 CE. J Volcanol Geotherm Res 215–216:8–25. https://doi.org/10.1016/j.jvolgeores.2011.11.009
Swanson DA, Rose TR, Mucek AE, Garcia MO, Fiske RS, Mastin LG (2014) Cycles of explosive and effusive eruptions at Kīlauea volcano, Hawaiʻi. Geology 42:631–634. https://doi.org/10.1130/G35701.1
Swanson DA, Houghton BF (2018) Products, processes, and implications of Keanakākoʻi volcanism, Kīlauea Volcano, Hawaiʻi. In: Poland MP, Garcia MO, Camp VE, Grunder A (eds) Field Volcanology: A Tribute to the Distinguished Career of Don Swanson. Geol Soc Am Special Pap 538:159–190. https://doi.org/10.1130/2018.2538(07)
Trusdell FA, Hungerford JDG, Stone JO et al (2018) Explosive eruptions at the summit of Mauna Loa: lithology, modeling, and dating. In: Poland MP, Garcia MO, Camp VE, Grunder A (eds) Field Volcanology: A Tribute to the Distinguished Career of Don Swanson. Geol Soc Am Special Pap 538:325–349. https://doi.org/10.5066/P144PUJA
van Helden KM, Schmith J, Downs DT (2024) Vesicularity, grain size, and grain shape of basaltic pyroclasts from Kīlauea and Mauna Loa volcanoes, Island of Hawaiʻi. US Geol Surv data release. https://doi.org/10.5066/P144PUJA.
Vergniolle S, Jaupart C (1986) Separated two-phase flow and basaltic eruptions. J Geophys Res 91:12842–12860
Vergniolle S, Jaupart C (1990) Dynamics of degassing at Kilauea volcano. Hawaii J Geophys Res 95:2793–2809
Vergniolle S (1996) Bubble size distribution in magma chambers and dynamics of basaltic eruptions. Earth Planet Sci Lett 140:269–279

Publisher's Note